J. Fluid Mech. (2009), *vol.* 628, *pp.* 395–425.
doi:10.1017/S0022112009006375 Printed in the United Kingdom

A mechanism of formation of multiple zonal jets in the oceans

P. BERLOFF[1,2]†, I. KAMENKOVICH[3] AND J. PEDLOSKY[1]

[1]Physical Oceanography Department, Woods Hole Oceanographic Institution, MA 02543 508/289-2462, USA

[2]Grantham Institute for Climate Change and Department of Mathematics, Imperial College, London SW7 2AZ, UK

[3]RSMAS, University of Miami, Coral Gables, FL 33146, USA

(Received 4 July 2008 and in revised form 26 January 2009)

Multiple alternating zonal jets observed in the ocean are studied with an idealized quasigeostrophic model of flow in a zonal channel. The jets are maintained by the eddies generated by the imposed, supercritical background flow. The formation, nonlinear dynamics and equilibration of the jets are explained in terms of linear stability arguments and nonlinear self-interactions of the linear eigenmodes. In the proposed mechanism, energy of the background flow is released to the primary instability mode with long meridional and short zonal length scales. This mode undergoes secondary, transverse instability that sets the meridional scale of the emerging multiple zonal jets. This instability channels energy into several weakly damped zonal eigenmodes that amplify the jets. The emerging jets feed back on the instabilities through the partial meridional localization of the most unstable eigenmodes.

1. Introduction

1.1. *Background*

The principal phenomenon studied in this paper is the formation of multiple, alternating zonal jets in the oceans. Solid observational (Hogg & Owens 1999; Maximenko, Bang & Sasaki 2005; Ollitrault *et al.* 2006; Huang *et al.* 2007; Sokolov & Rintoul 2007; Herbei, McKeague & Speer 2008; Ivanov, Collins & Margolina 2008; Maximenko *et al.* 2008; Schlax & Chelton 2008) and numerical (Sinha & Richards 1999; Nakano & Hasumi 2005; Richards *et al.* 2006; Huang *et al.* 2007; Kamenkovich, Berloff & Pedlosky 2008) evidence of these jets has emerged over the last few years. It is plausible that these jets are dynamically similar to those observed in the atmospheres of giant gas planets, such as Jupiter (Galperin *et al.* 2004).

Oceanic multiple zonal jets are *latent* jets, because they are comparable to or even weaker than the associated mesoscale eddies, which tend to mask the jets in instantaneous flow snapshots. Also, the oceanic multiple jets are perturbations on the background flows such as the mid-latitude gyres and the Antarctic Circumpolar Current. Typical velocities of the time-mean oceanic jets are a few centimetres per second, which makes them prominent features of the deep-ocean circulation. The meridional wavelength of the jets is 150–300 km, and overall it decreases at higher

† Email address for correspondence: pberloff@whoi.edu

latitudes. The vertical structure as well as the seasonal and interannual variabilities of the jets are poorly known. Atmospheric multiple zonal jets are *manifest* jets, because they are substantially stronger than the associated eddies. On giant gas planets, such as Jupiter, the jets easily manifest themselves as alternating stripes of different colours.

The theoretical cornerstone of the multiple-jet studies was laid by Rhines (1975), who, from the analysis of decaying barotropic turbulence, argued that the meridional scale of the jets (a.k.a. Rhines scale) is determined by a balance between the nonlinear advection and the linear meridional advection of the planetary vorticity. (The Rhines scale is commonly thought of as the physical scale at which the inverse energy cascade in the turbulence is 'arrested' by the propagating Rossby waves. However, there are arguments that most of the cascading energy overcomes the 'arrest' and continues to cascade up to the largest scales (Huang & Robinson 1998; Sukoriansky, Dikovskaya & Galperin 2007).) Since then, nearly all theories of the jets invoke both nonlinearity of the flow and the meridional gradient of the Coriolis parameter (i.e. the β-effect) as the fundamental aspects. However, the required degree of nonlinearity is uncertain, and it has been argued that the barotropic jet can be a weakly nonlinear phenomenon (Manfroi & Young 1999, 2002). Also, it has been argued that the jets emerge only if the β-effect exceeds a critical threshold, which depends on latitude, the first Rossby deformation radius and the intensity of the energy cascade (Smith 2004; Theiss 2004). Finally, with the latitude-dependent planetary-vorticity gradient, an equatorward energy cascade has been proposed that should amplify the jets at the low latitudes (Theiss 2004).

Since the pioneering work of Williams (1978), who looked at an idealized but global model of the barotropic atmosphere, particular attention has been paid to the equilibrated barotropic dynamics. There, the barotropic jets emerge in forced-dissipative regimes driven by the spatially homogeneous, small-scale random forcing. Such forcing is assumed to represent interactions of the barotropic mode with the transient baroclinic eddies. The energy spectrum corresponding to the barotropic multiple-jet regime is strongly anisotropic (e.g. Vallis & Maltrud 1993; Chekhlov *et al.* 1996; Danilov & Gryanik 2004; Danilov & Gurarie 2004; Galperin *et al.* 2004), and the spectral nonlinear interactions are significantly non-local (Balk, Nazarenko & Zakharov 1990). From the stochastic structural stability approach, it is argued that the barotropic jets are the preferred growing structures excited by the imposed stochastic forcing (Farrell & Ioannou 2007, 2008).

Baroclinic jet components, baroclinic dynamics and interactions between the barotropic and baroclinic vertical modes are poorly understood, because they require more complex models with several vertical degrees of freedom. In a two-layer model of a baroclinically unstable background flow, multiple zonal jets emerge and persist for a long time (Panetta 1993, hereafter P93). In the explored range of parameters, P93 finds that meridional scaling of these jets is consistent with the Rhines scale and that the jets are maintained by divergence of the momentum rather than buoyancy eddy flux. The results of P93 have been extended towards multiple zonal jets in a wind-driven, zonal-channel model (Treguier & Panetta 1994). Some other studies focus on transitions between the one- and two-jet regimes (Lee 1997) and on the truncated P93-like model (Kaspi & Flierl 2007). Finally, it is suggested that, in the presence of bottom friction, baroclinic jets have baroclinic–barotropic interactions that break down the inverse cascade arguments (Thompson & Young 2007).

It has been proposed that the multiple jets can be interpreted kinematically, in terms of the "potential vorticity (PV) staircase" conjecture (Baldwin *et al.* 2007; Dritschel & McIntyre 2008), which stems from the inhomogeneous mixing argument of McIntyre

(1982). The underlying idea of the conjecture is that the cores of the (prograde) eastward jets tend to act as narrow material transport barriers that separate broad zonal bands characterized by intense meridional mixing of material by the eddies.

Finally, there are relatively few studies of multiple zonal jets in idealized closed basins (Berloff 2005; Kramer *et al.* 2006; Nadiga 2006), and dynamical differences between the zonal-channel and closed-basin jets remain poorly understood.

To summarize, our present theoretical understanding of the multiple zonal jets is dominated by the 'kinematic' and 'spectral' approaches. The former one talks about relatively well-mixed eddy surf zones separated by the meridional transport barriers that constitute the underlying kinematical template of the multiple jets. The latter one focuses on the anisotropic inverse energy cascade that stops at some scale and feeds the multiple jets. It is still unclear which of the proposed ideas apply to the ocean and atmosphere, because the underlying theoretical models remain highly idealized. The essential and novel part of our present work is that we promote linear stability analysis and nonlinear self-interactions of the critical eigenmodes as the arguments underpinning dynamics of the multiple jets. Also, in many aspects the model that we analyse is more realistic than most of the previously studied theoretical models.

1.2. *Statement of the problem*

Our principal hypothesis is that the oceanic jets are driven by the intrinsic nonlinear dynamics associated with mesoscale geostrophic eddies, rather than by inhomogeneities of the oceanic boundary conditions. We focus on a variation of the classical idealized model of the multiple zonal jets in a zonal channel (e.g. in P93) but choose the model parameters with guidance from the eddy-resolving model of the North Atlantic that simulates a set of such jets (Kamenkovich *et al.* 2008; hereafter KBP08). In this solution there are zonal jets everywhere, but we focus on two distinct sets of pronounced multiple jets in the two regions: one region includes northern part of the subtropical gyre and southern part of the subpolar gyre, and the other region includes southern part of the subtropical gyre. In both regions the background flow is upper-ocean-intensified and predominantly zonal; in the former region it is eastward, whereas in the latter one it is westward. Therefore, in our idealized model, the eddies and, thus, the jets are maintained by either *eastward*-background (EB) or *westward*-background (WB) flows, which correspond to different parts of the North Atlantic wind-driven gyres. (In the idealized studies of the atmospheric jets, only EB flows are considered, because of the generic equator-to-pole decrease of temperature associated with them.) We calculate fully nonlinear solutions and focus not only on their equilibrated states but also on their spin-up from the perturbed state of rest. Our focus is on the flow patterns and eddy/large-scale interactions, and the goal is to explain the mechanism responsible for formation of the jets.

The main distinction of this work from the previous studies is in the use of linear stability arguments. This approach is different from the 'arrested' inverse cascade and 'PV staircase' ideas discussed in previous section.

1.3. *Ocean model*

This is the model of jet formation in an idealized zonal background flow, which can represent a mid-latitude gyre interior, away from meridional boundaries, or the Antarctic Circumpolar Current. The jets, driven by instabilities of the prescribed supercritical background velocity with vertical shear, are simulated in zonally periodic channel with vertical walls and flat bottom. Uniformity of the background flow and

absence of the bottom topography allow us to avoid additional length scales of the problem. Here, the motivation is to establish the simplest, but physically relevant, starting point; more physical complexity can be systematically added later on. Overall, the model is close to that of P93.

The meridional width of the channel is mostly $L_y = 1800$ km, but some solutions with $L_y = 3600$ km are also discussed. The channel is zonally periodic with the period $L_x = 2\,L_y$. The background planetary vorticity gradient is $\beta = 2 \times 10^{-11}\,\mathrm{m^{-1}\,s^{-1}}$, and the mid-channel (45 °N) Coriolis parameter is $f_0 = 0.83 \times 10^{-4}\,\mathrm{s^{-1}}$. The bottom friction $\gamma = 2 \times 10^{-8}\,\mathrm{s^{-1}}$ is small and only 6 % of the energy is dissipated by the bottom. Most of the energy is dissipated by the lateral friction, which parameterizes effects of unresolved eddies; the eddy viscosity is $\nu = 100\,\mathrm{m^2\,s^{-1}}$. Stratification is represented by two stacked isopycnal layers with the thicknesses $H_1 = 1$ km and $H_2 = 3$ km, starting from the top. The stratification parameters are

$$S_1 = \frac{f_0^2}{H_1\, g_1'}, \quad S_2 = \frac{f_0^2}{H_2\, g_1'}, \tag{1}$$

where g_1' is reduced gravity associated with the density jump across the internal interface. We chose g_1' so that the first baroclinic Rossby deformation radius $Rd_1 = g_1'\sqrt{H_1 H_2}/f_0\sqrt{H_1 + H_2}$ is 25 km.

The quasigeostrophic PV equations (Pedlosky 1987) for two dynamically active isopycnal layers are

$$\frac{\partial q_1}{\partial t} + J(\psi_1, q_1) + \beta\,\frac{\partial \psi_1}{\partial x} = \nu\nabla^4\psi_1, \tag{2}$$

$$\frac{\partial q_2}{\partial t} + J(\psi_2, q_2) + \beta\,\frac{\partial \psi_2}{\partial x} = \nu\nabla^4\psi_2 - \gamma\nabla^2\psi_2, \tag{3}$$

where the layer index starts from the top; $J(,)$ is the Jacobian operator; and the terms with ν and γ are the lateral and bottom friction, respectively. Isopycnal PV anomalies q_i are related to velocity streamfunctions ψ_i through the elliptic, PV inversion sub-problem:

$$q_1 = \nabla^2\psi_1 + S_1\,(\psi_2 - \psi_1), \tag{4}$$

$$q_2 = \nabla^2\psi_2 + S_2\,(\psi_1 - \psi_2). \tag{5}$$

The isopycnal flow velocity components are found from the velocity streamfunction:

$$u_i = -\frac{\partial \psi_i}{\partial y}; \quad v_i = \frac{\partial \psi_i}{\partial x}. \tag{6}$$

The dynamical equations are actually solved either in their original, isopycnal-layer form or in terms of their vertical-mode equivalence (McWilliams 2006). No-slip lateral-boundary conditions are used on the lateral walls. The mass and momentum constraints are imposed following McWilliams (1977).

The forcing in the governing equations is introduced through the imposed, background vertical velocity shear (e.g. Haidvogel & Held 1980; Panetta 1993):

$$\Psi_i = -U_i\,y, \quad \psi_i \longrightarrow \Psi_i + \psi_i, \tag{7}$$

where U_i are the background zonal-velocity parameters of the problem. In the EB and WB flow regimes, $U_1 = 6$ and -3 cm s^{-1}, respectively; and U_2 is zero. The background flow is linearly unstable, as suggested by the classical Phillips problem (e.g. Pedlosky 1987). Given (7), the governing equations are rewritten with respect to perturbations, ψ_i and q_i, around the background flow.

The governing equations (2)–(7) are discretized with second-order finite differences, so that formulation of the Jacobians is PV-conserving. The prognostic equations are marched in time with the leapfrog scheme and 0.5 hour time step, and the elliptic PV inversion sub-problem is solved for the corresponding velocity streamfunctions on each time step, by a direct solver. The horizontal grid, with 512×257 points, has uniform resolution of 7 km. Statistically equilibrated regimes are reached after 20–40 years of integration.

Equilibrium solutions of the nonlinear flow have well defined multiple jets (figure 1). The jets have a relatively strong barotropic component. The eastward jets are faster and narrower than the westward jets. The EB flow has stronger jets because of the stronger critical shear. In the EB flow barotropic and baroclinic jet components are in phase with each other, whereas in the WB flow they oppose each other. As a result of this behaviour, in the EB/WB flow deep-ocean jets are weaker/stronger than the upper-ocean jets.

2. Spin-up

We begin with the analysis of the fully nonlinear spin-up of flow from the state of rest, which is seeded with random small-amplitude perturbations. The spin-up process provides insights which we later use for explaining the underlying mechanism of the multiple-jet formation.

At the first stage of the spin-up, the structure of the emerging alternating meridional jets (figure 2*a*) is very consistent with the primary instability mode (a.k.a. 'noodles') predicted by the linear stability analysis (see § 3.2). The mode is a result of the baroclinic instability, and its zonal scale depends on the baroclinic deformation radius. Motion in the 'noodles' is perpendicular to the background flow; hence they maximize extraction of the available potential energy from the background flow. Also, in figure 2(*a*) there are 'braids' that distort the noodles: we associate them with weakly damped, large-scale eigenmodes of the model (also discussed in § 3.2). We checked that if the initial perturbation is chosen in the form of the linear noodles; then the large-scale eigenmodes are not significantly excited, because they are initially absent.

At the second stage of the spin-up, the noodles succumb to the secondary instability discussed in § 3.3. This process is manifested in figure 2(*b*) by the emergence of flow structures with the meridional scale of the jets. This instability imposes the meridional scale of the future multiple jets. Also, seen on this stage is the emerging zonal eigenmode, which is discussed in § 3.4. This eigenmode feeds the emerging zonal jets.

The third spin-up stage is characterized by amplification of the emerging multiple jets and by continuing meridional localization of the noodles by the emerging jets (figure 2*c*), until the flow equilibrates at a finite amplitude. The equilibration can be interpreted as significant meridional localization of the flow instabilities, as we show in § 3.6. The third spin-up stage is more pronounced in the zonal-channel situation, because there are zonal eigenmodes available which strongly amplify the jets. In the closed-basin extension of the model, the jets are weaker and more latent; hence the third spin-up stage is less pronounced (Berloff, Kamenkovich & Pedlosky 2009).

Comparison of the spin-up experiments with oceanic observations is problematic, since the ocean not only stays close to the equilibrated state but is also affected by the seasonal and interannual variabilities. However, the emergence of the noodles, followed by the emergence of zonal currents, is consistent with observations of seasonally modulated instabilities of the South Pacific subtropical countercurrent (Qiu, Scott & Chen 2008; Farrar 2008, personal communication). Also, qualitatively

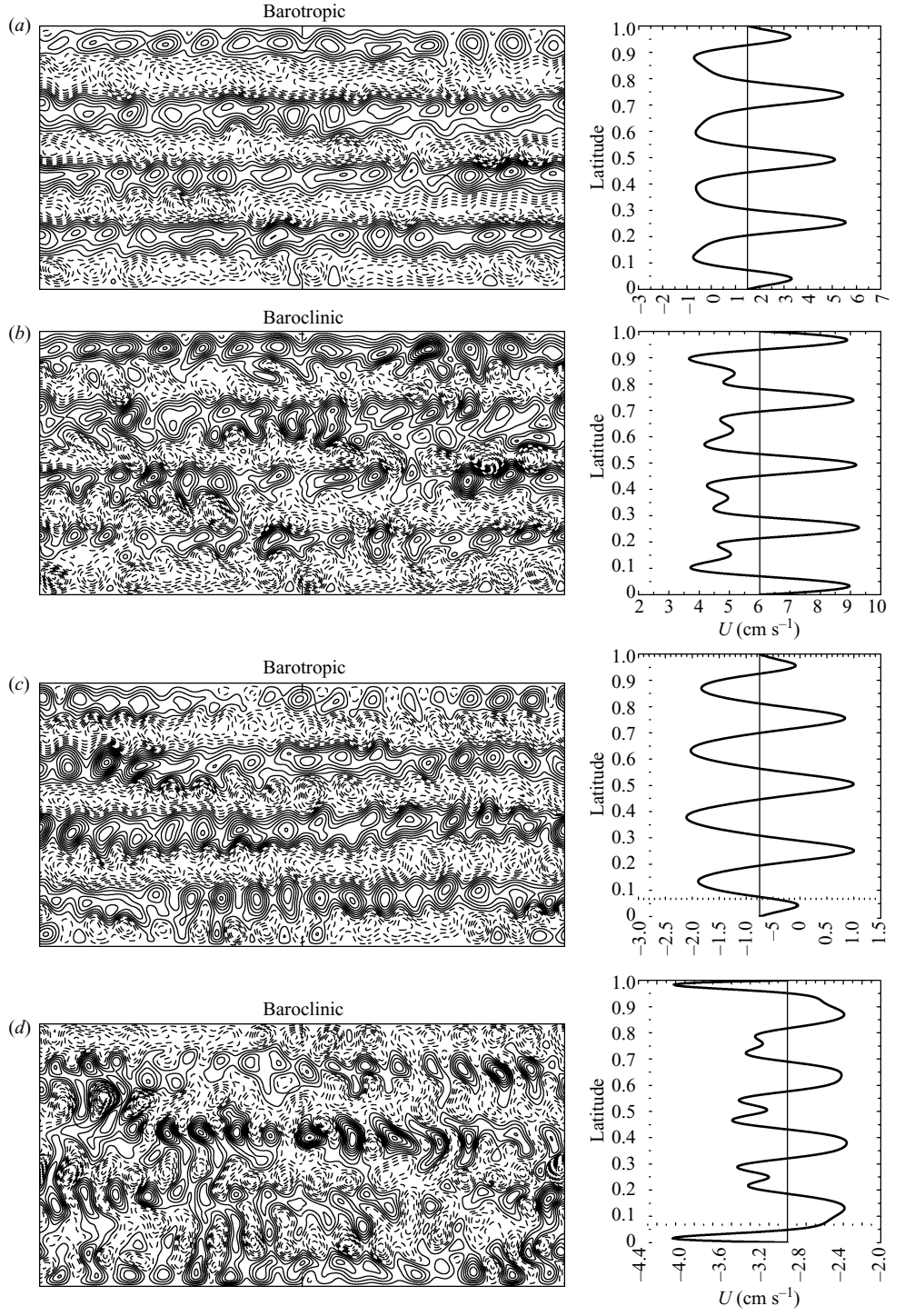

FIGURE 1. Multiple-jet flow in the two-layer zonal channel. Instantaneous (*a*) barotropic and (*b*) baroclinic velocity streamfunctions in the reference EB flow (CI = 2 Sv). The corresponding time-mean zonal velocity profiles are shown in the right panels. Panels (*c*) and (*d*) show the same quantities as the upper panels but for the reference WB flow (CI = 1 Sv). Straight lines indicate the background velocities. Latitude values are normalized by the width of the channel ($L_y = 1800$ km $= 72Rd_1$).

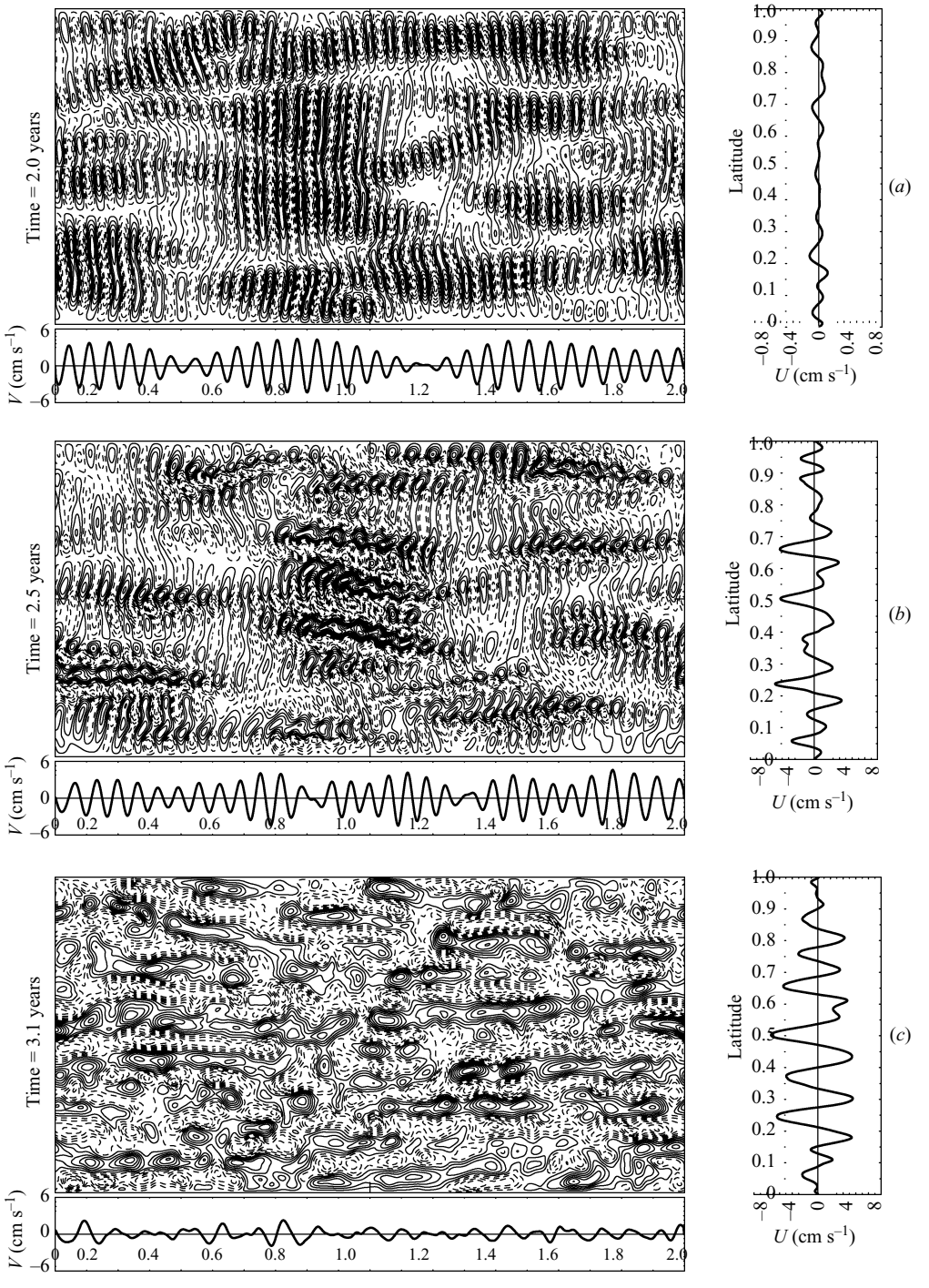

FIGURE 2. Spin-up of the multiple jets. Instantaneous upper-ocean streamfunction is obtained (*a*) after two years of the model integration starting from small random perturbations, (*b*) 200 days later and (*c*) another 200 days later; CI are (*a*) 0.4 Sv and (*b*, *c*) 5 Sv. The reference EB flow solution is obtained in the broad channel. Panel to the right of each streamfunction field shows the corresponding zonally averaged zonal velocity, and panel below the streamfunction field shows meridionally averaged meridional velocity.

similar behaviours are reported in spin-up experiments with the North Atlantic eddy-resolving model (KBP08).

3. Linear stability problem

In this section we present a theoretical framework that interprets modification of the flow on each of the main three stages of the spin-up. Our approach is to apply a linear stability analysis on each of these stages.

3.1. *Formulation*

The linear stability analysis considered in this section is an extension of the classical works (Phillips 1956; Pedlosky 1975*b*). The linearized governing equations of the two-layer dynamics are

$$\frac{\partial q_1}{\partial t} + J(\Psi_1, q_1) + J(\psi_1, Q_1) + \beta\,\psi_{1x} = \nu\nabla^4\psi_1, \tag{8}$$

$$\frac{\partial q_2}{\partial t} + J(\Psi_2, q_2) + J(\psi_2, Q_2) + \beta\,\psi_{2x} = \nu\nabla^4\psi_2 - \gamma\nabla^2\psi_2, \tag{9}$$

where Q_i and Ψ_i are the background PV and velocity streamfunction, respectively.

We consider three types of the background flow: (i) zonal, meridionally uniform flow; (ii) combination of (i) with meridional, zonally periodic flow; and (iii) zonal, meridionally non-uniform flow. These types correspond to the flows that are present at the end of each stage of the spin-up. The first flow type, given by (7), is the simplest one – its critical eigenmode describes the primary instability, discussed in § 3.2. This problem also yields weakly damped and zonally uniform eigenmodes, important for the multiple-jet formation mechanism, that are discussed in § 3.4. The second flow type is dictated by the critical eigenmodes of the first flow type,

$$\Psi_i = -U_i\,y + \int_0^x V_i(x)\,\mathrm{d}x, \tag{10}$$

and it yields the critical eigenmode describing the secondary instability, discussed in § 3.3. Here, we consider meridional velocity components that are zonally periodic:

$$V_i(x) \longrightarrow A_v\,V_i\,\cos(2\pi x/L_0 + \Phi_i). \tag{11}$$

Here, V_i, L_0 and Φ_i are given by the primary instability pattern; the amplitude A_v is a new parameter of the problem, which is given by the strength of the noodles emerging in spin-up experiments (§ 4.4). Finally, with the third flow type, we analyse the stability of the finite-amplitude zonal jets:

$$\Psi_i = -U_i\,y - A_u\int_0^y u_i(y)\,\mathrm{d}y. \tag{12}$$

As the amplitude of these jets A_u increases, as a part of the spin-up process, not only do the noodles become distorted and partially meridionally localized on the jets, but also they split into three distinct types of the eigenmodes, discussed in §§ 3.5 and 3.6.

The linearized equations are Fourier transformed in time and in either one or both horizontal directions (see the Appendix). The direction that is not Fourier transformed is discretized with second-order finite differences, and the spatial resolution is kept the same as in the full nonlinear model. We tested that the outcome is not sensitive to further refinement of the spatial grid. For the flow of the third type, a no-slip boundary condition is applied on the zonal boundaries. The discretized equations are

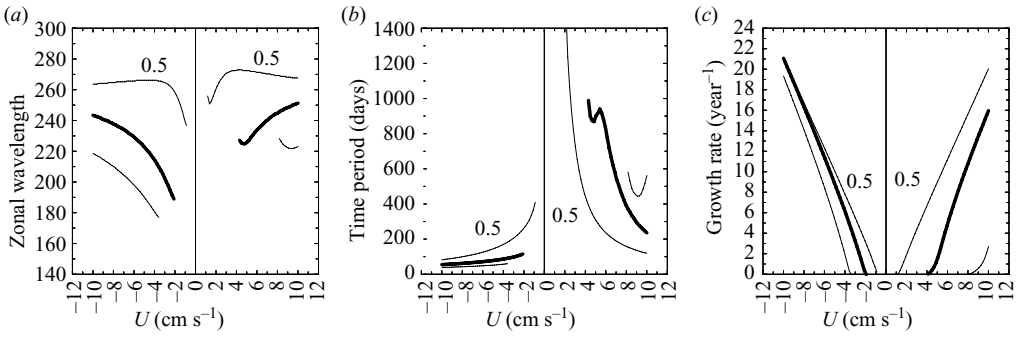

FIGURE 3. Properties of the most unstable eigenmode (i.e. noodles) growing on the uniform zonal flow in the unbounded domain: dependence on the planetary vorticity gradient, β. (*a*) Zonal wavelength, (*b*) time period and (*c*) growth rate as functions of the upper-ocean background velocity. On each panel, thick curve corresponds to the reference value of $\beta = 2 \times 10^{-11}\,\mathrm{m^{-1}\,s^{-1}}$. There are three values of β considered: 0.5, 2 and $4 \times 10^{-11}\,\mathrm{m^{-1}\,s^{-1}}$ (curves corresponding to the lowest value are labelled by '0.5').

solved numerically as the generalized eigenvalue problem. The solutions are obtained in terms of the eigenmode patterns and the eigenvalues, which specify growth rates and temporal frequencies of the eigenmodes.

3.2. *Uniform background flow: unbounded domain*

Marginal stability curves corresponding to uniform zonal flow of variable strength are shown in figure 3, and the typical dispersion relationships are shown in figure 4. Overall, the dispersion relationship is that of the classical Rossby waves modified by the background shear and damping. Without lateral viscosity and bottom friction and with equal layer depths, this is the Phillips problem (Pedlosky 1987). In both EB and WB flows and depending on the parameters of the problem, the critical eigenmode (figure 4) has relatively large zonal wavenumbers k which correspond to the wavelength of 180–270 km. Given $Rd_1 = 25$ km, this is 7–11 Rd_1 – noticeably longer than $2\pi Rd_1$. The critical meridional wavenumbers l are always equal to *zero*; hence the critical eigenmode can be characterized as a set of *meridional alternating jets*: following Pedlosky (1975*b*) we refer to such a pattern as *noodles*. In the supercritical EB/WB flow, the phase of the critical eigenmode always propagates to the east/west, and the corresponding eigenperiods are interannual/intermonthly. Regardless of the background shear, there are also very weakly damped eigenmodes with small k and l – they can be easily excited by transient forcing. In the next section we argue that some of the eigenmodes with $k = 0$ (zonal eigenmodes) and small l significantly contribute to the multiple jets.

Increasing the speed of the background flow results in shorter time periods, longer zonal wavelengths and larger growth rates of the noodles (figure 3). We also studied the dependence of noodles on ν, γ and β. The magnitude of the critical background flow strength increases with ν and β (figure 3*c*); in the EB/WB flow it weakly increases/decreases with γ. The zonal eigenperiod $2\pi/k$ increases moderately with ν and very weakly with γ. This is because lateral friction, unlike the bottom drag, acts selectively on the smaller length scales and, thus, moves the stability threshold to larger length scales. The time period is largely insensitive to ν; variation of γ changes it noticeably only in the EB flow, so that larger friction implies shorter period. Increasing β decreases the zonal eigenperiod for both background flow directions – this makes the noodles narrower. The corresponding time period becomes even

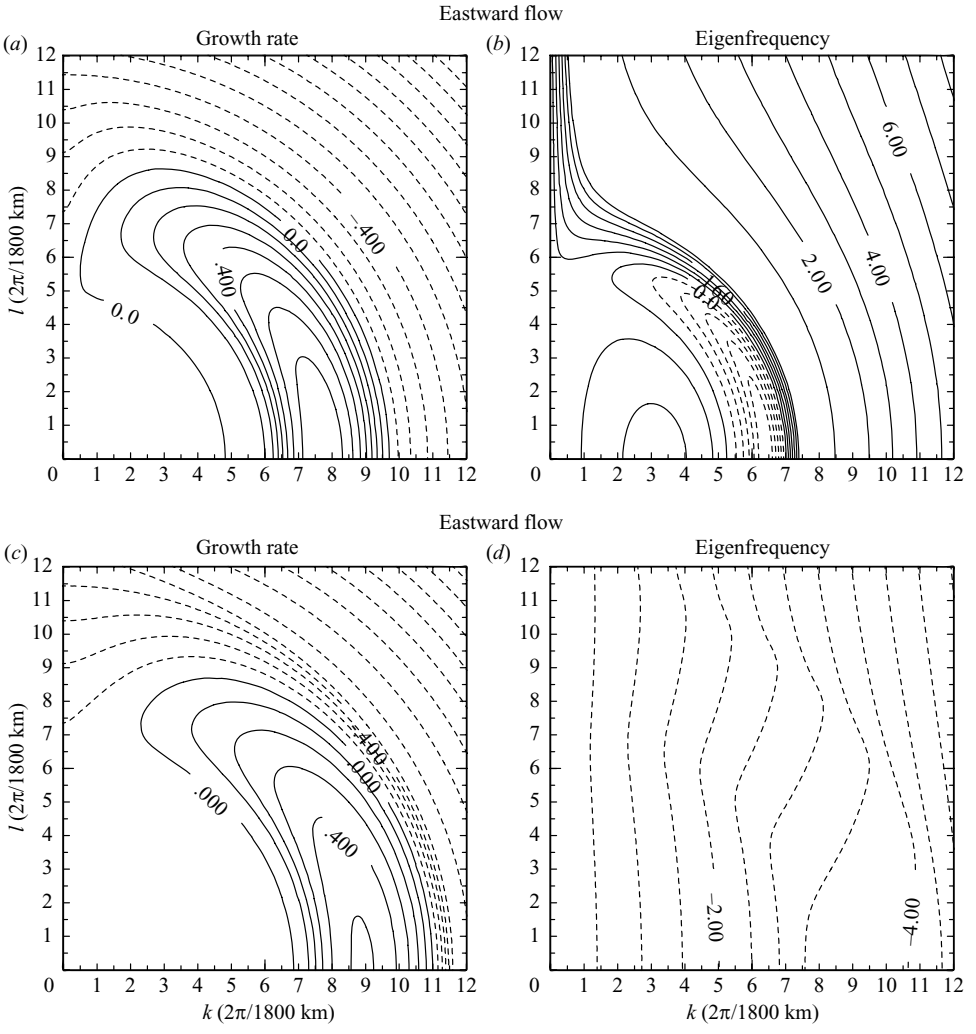

FIGURE 4. Dispersion relationship of the linear stability problem: uniform zonal flow in the unbounded domain. The upper row of panels shows (*a*) growth rate and (*b*) eigenfrequency of the reference EB flow as functions of the zonal (k) and meridional (l) wavenumbers. The lower row of panels shows the same values but for the reference WB flow. Contour intervals: (*a*,*c*) CI = 0.1 year^{-1}; (*b*) CI = 0.04 and 1.0 year^{-1} for the small and large eigenfrequencies, respectively; and (*d*) CI = 0.5 year^{-1}. Positive/negative contours in the right panels correspond to the phase lines propagating to the east/west.

longer/shorter in the EB/WB flow, thus increasing the asymmetry between the EB and WB noodles.

In the real ocean, the noodles are likely to be distorted by the background flow and planetary vorticity inhomogeneities, as well as by the large-scale transient variability. In particular, in figure 2(*a*) there are braids that distort the noodles: we associate them with weakly damped eigenmodes of the model. These eigenmodes occupy the lower left corners of the dispersion diagrams in figure 4. In addition to all of these inhomogeneous aspects, the noodles are distorted by the jets themselves as a part of the feedback of the jets on the eddies (§ 3.5).

Finally, the analysis of this section is extended from the unbounded domain to the zonal channel. The stability properties of the corresponding flow are found to be very similar: details of the zonal-channel noodles are accurately predicted by the unbounded-domain analysis. In the free-slip channel, the critical (i.e. with the largest growth rate) mode is exactly the sum of the two critical eigenmodes of the unbounded domain, with $\pm l_{crit}$. Such a mode propagates in zonal direction only. In the no-slip channel, which is in the focus of this study, the above mode is modified near the boundaries. We find that this modification has little impact on other properties of the mode.

To summarize, generation of the flow pattern with long-range meridional correlations is a very robust phenomenon, but details of this pattern are somewhat sensitive to the background flow and other external parameters.

3.3. *Secondary instability*

The finite-amplitude noodles are unstable to the transverse secondary instability, which is consistent with the one seen in the spin-up solutions (§ 2.4). Secondary instabilities of different flows have been studied in the past (e.g. Orszag & Patera 1983; Bonfigli & Kloker 2005; Stern & Simeonov 2005), and here we extend the work by Pedlosky (1975*b*) by adding the background flow to the noodles and by relating the results to the multiple-jet problem.

For the corresponding linear stability problem, the flow consists of the ensemble of finite-amplitude noodles, given by the primary stability analysis, that are added to the uniform background flow (figure 5*a*, *e*). (Here, the argument is similar to Manfroi & Young (2002), but the background-flow and baroclinic effects are taken into account.) The amplitude of the noodles is provided by the spin-up solutions at the end of the first spin-up stage, but for the theoretical purposes we treat their amplitude as a free parameter, as in (11). The noodles are kept 'frozen' in time; that is their slow zonal propagation is not taken into account, for simplification of the linear analysis. We verified that this simplification does not introduce large errors by calculating growing and breaking noodles in the fully nonlinear model. In these calculations, the initial noodles were perturbed with anomalies of different length scales. Here, we find that the meridional scale of the fastest growing transverse mode is similar to the meridional scale predicted by our linear analysis.

The secondary instability, given by the fastest growing eigenmode, is meridionally periodic, with the scale corresponding to the multiple zonal jets (figure 5). In the zonal direction, the secondary eigenmodes are not trapped by the individual noodles, as indicated by their amplitudes that never approach zero. The zonal wavelength of the eigenmode amplitude is half of the wavelength of the noodles, thus indicating that the corresponding northward and southward meridional jets have the same impacts on the eigenmode pattern. Other eigenmode properties differ for the EB and WB flows: in the former case, the eigenmode is characterized by the 'checkerboarded' velocity streamfunction (figure 5*b*), whereas in the latter case the streamfunction is 'striped' (figure 5*f*). This is because the WB eigenmode is characterized by weaker zonal variation of the phase. As can be seen in their zonal averages, both the checkerboarded and striped patterns have obvious contributions of the dominant, primary zonal eigenmodes. Hence, the transverse instability provides an efficient mechanism of the energy transfer from the meridional directly to zonal motions. (Such spectrally non-local energy transfer is observed in the mesoscale eddy fields (Qiu *et al.* 2008).)

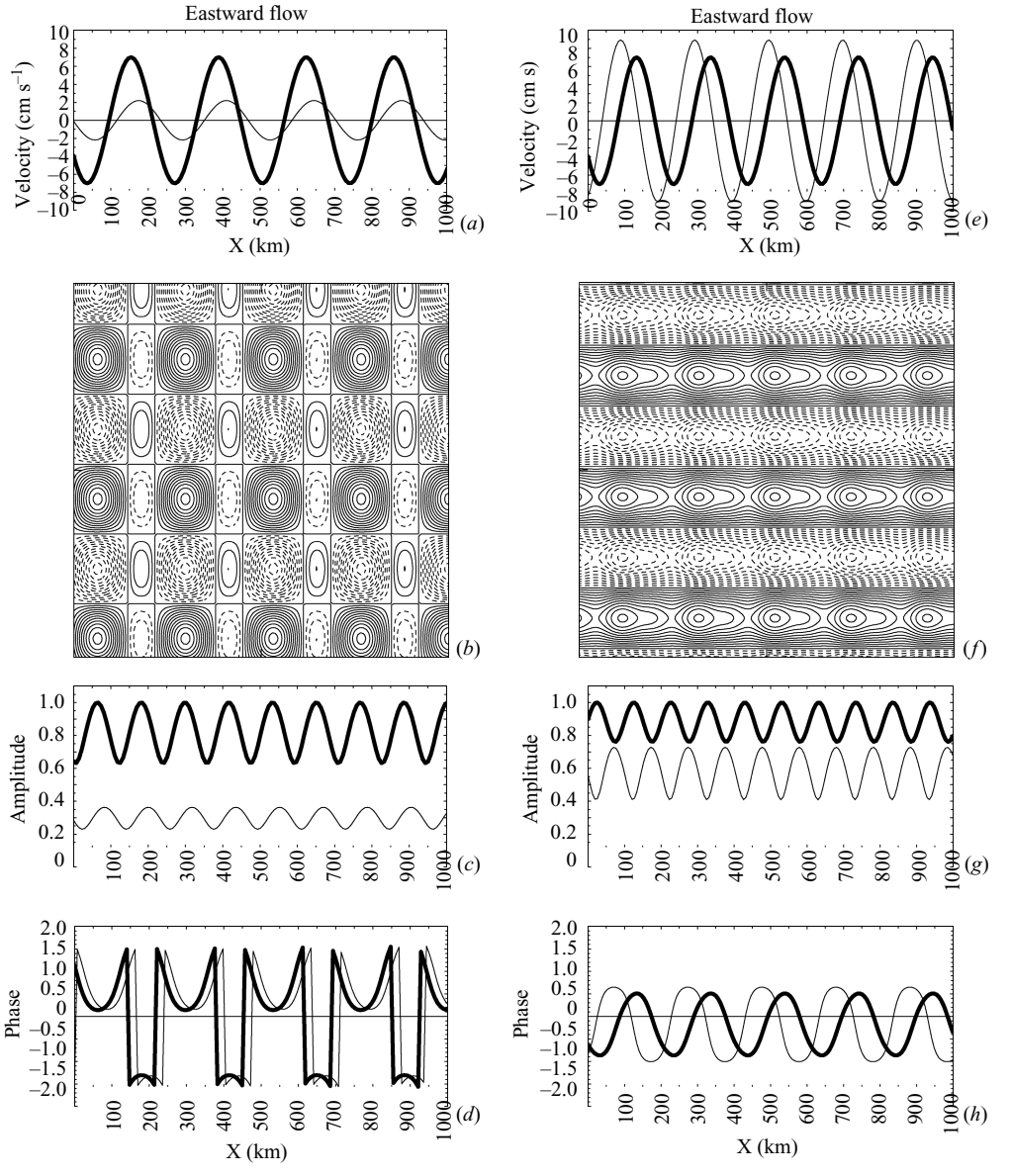

FIGURE 5. Critical eigenmodes of the finite-amplitude noodles. Left/right column of panels corresponds to the EB/WB flow solution. (a, e) Meridional velocity of the background noodles in the upper- (thick) and deep-ocean (thin curve) isopycnal layers. (b, f) Upper-ocean velocity streamfunction (arbitrary amplitude). (c, g) Amplitude (normalized by its upper-ocean maximum value) and (d, h) phase of the zonal component of the critical eigenmode.

The meridional length scale of the secondary instability, that is the scale of the fastest growing eigenmode, which sets the meridional width of the jets, depends on the amplitude of the noodles but saturates when the amplitude of the noodles becomes comparable with the amplitude of the background flow (figure 6*a*). If the amplitude approaches zero, then the meridional length scale increases to infinity, because instabilities of the background flow with infinitesimal noodles are the noodles

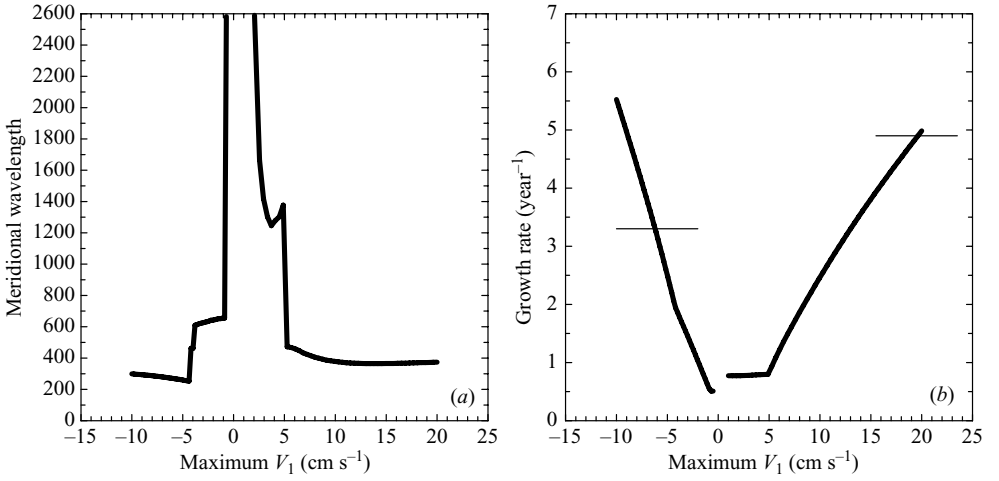

FIGURE 6. Stability properties of the finite-amplitude noodles. (*a*) Meridional wavelength and (*b*) growth rate of the critical eigenmodes of the EB and WB flow solutions. Positive/negative values of the maximum upper-ocean meridional velocity, V_1, indicate EB/WB flows. Thin horizontal lines in (*b*) indicate growth rates of the infinitesimal noodles.

themselves. If the amplitude becomes 1.5–2 times larger than the background zonal flow, then the meridional length scale saturates at about 300–400 km (i.e. 12–16 Rd_1), which is consistent with the emerging multiple zonal jets.

Can the transverse instability be dominated by larger length scales associated with the weaker noodles? (For instance, figure 6*a* suggests that critical instabilities of the WB flow noodles with the velocity amplitude of about 1.5–4.0 cm s^{-1} have the meridional length scale of about 600 km.) The answer is no, because critical instabilities of the weaker noodles have growth rates that are smaller than the growth rates of the noodles themselves (figure 6*b*). This implies that, before such weakly growing eigenmodes grow to finite amplitudes, the noodles themselves will grow to a larger amplitude, and then they will develop narrower zonal jets. We confirmed this by fully nonlinear calculations, as those described in the beginning of this section. Thus, the secondary instability eventually overcomes the primary instability pattern because of the faster growth rates of the former rather than because of the potential saturation of the primary instability by the nonlinearity.

Finally, we find that eigenperiods of the critical eigenmodes are infinitely large. Thus, the corresponding phase velocity is zero, and therefore the secondary instability pattern does not propagate in space. This also implies that the instability pattern does not propagate meridionally. Hence the multiple zonal jets are pinned to their locations and are not averaged out in the time mean.

To summarize, meridional scale of the multiple zonal jets is set by the instability of the noodles emerging on the background flow. The corresponding critical eigenmode efficiently projects on the dominant zonal mode that acts as the template for the emerging jets.

3.4. *Zonal eigenmodes*

In this section we consider a special set of the eigenmodes discussed in previous section; some of the zonally uniform eigenmodes ($k = 0$) significantly contribute to the multiple zonal jets. These eigenmodes, occupying the lower left corner of the dispersion diagrams (e.g. figure 4), are very weakly damped. The zonal eigenmodes

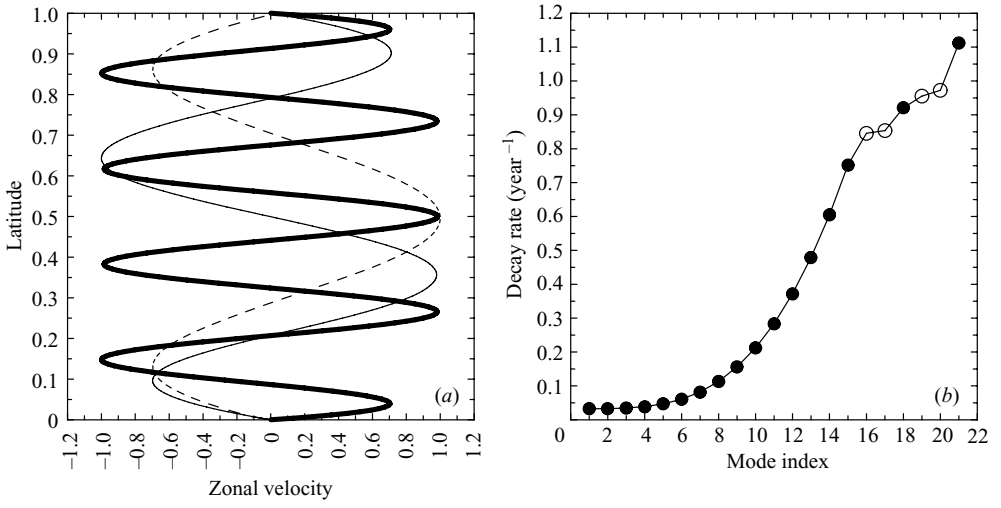

FIGURE 7. Zonal eigenmodes. (*a*) Upper-ocean zonal velocity profiles of the second (dashed), third (thin) and eighth zonal eigenmodes (thick curve); (*b*) decay rates of the first 20 zonal eigenmodes, ranked according to the increasing decay rate. The eigenmodes are calculated for the reference control parameters. Zonal velocities in (*a*) are normalized by their maximum absolute values. Filled/empty circles in (*b*) indicate predominantly baroclinic/barotropic eigenmodes.

predicted by the unbounded-domain analysis are modified by the zonal-channel boundaries (figure 7). The bounded eigenmodes preserve their weak decay rates, and hence the eigenmodes with fewer meridional lobes need weaker forcing to get excited. The spectrum of the bounded zonal eigenmodes is discrete. An important property of the zonal eigenmodes is that they do not depend on the background flow, as can be easily seen from the governing equations.

We order the zonal eigenmodes in terms of increasing decay rate. We find that the baroclinic component of the reference EB and WB solutions is dominated by the eighth mode. Half of the zonal eigenmodes (e.g. the third mode in figure 7*a*) have zonal velocity which is meridionally antisymmetric with respect to the middle of the channel. Such eigenmodes imply non-zero total viscous flux of the relative vorticity from the lateral boundaries into the channel interior. Therefore, they do not satisfy the momentum constraint imposed by the dynamics (McWilliams 1977). This explains why multiple-jet time-mean flows predicted by the full model have zonal velocity which is nearly symmetric around the middle latitude – they are dominated by the meridionally symmetric zonal eigenmodes. (There are special antisymmetric flow configurations that have no relative vorticity flux from the lateral boundaries, but, for reasons unknown to us, the dynamics do not favour antisymmetric flow contributions.) Decay rates of the zonal eigenmodes increase with the eigenmode index more than in the unbounded domain, so that the tenth eigenmode decays five times faster than the first eigenmode. This suggests that the full flow is likely to be dominated by relatively few zonal eigenmodes. In terms of their vertical structure, the zonal eigenmodes are all mixed; that is they are neither barotropic nor baroclinic. However, the important zonal eigenmodes (i.e. those with low index) have a ratio of their barotropic to baroclinic component which is either small (<0.1) or large (>10): such eigenmodes can be accurately (but not precisely) characterized as baroclinic and

barotropic, respectively. We find that the first dozen zonal eigenmodes with weak decay rates are baroclinic, and the barotropic eigenmodes of interest have higher indices.

How do the zonal eigenmodes contribute to the time-mean multiple jets? Let's consider a set of the $n = \overline{1, N}$ zonal eigenmode streamfunctions $\chi_n(y)$ that are ordered in terms of the increasing decay rate and are normalized by the energy norm. The observed, time-mean jet streamfunction can be represented as

$$\varphi = \sum_{1}^{N} C_n \chi_n, \tag{13}$$

where the set of C_n is the zonal mode spectrum and N is the number of meridional degrees of freedom. We define the scalar product of two streamfunction fields as

$$\{\phi\, \psi\} = \frac{1}{L_y} \int_0^{L_y} \phi(y)\, \psi(y)\, \mathrm{d}y. \tag{14}$$

Multiplication of (13) by each of the N zonal eigenmodes, yields the corresponding set of linear equations on C_n:

$$\{\varphi\, \chi_n\} = \sum_{m=1}^{m=N} C_n \{\chi_n\, \chi_m\}. \tag{15}$$

Scalar products of the zonal eigenmodes on the right-hand side of (15) are generally non-zero for $n \neq m$, because the eigenmodes are not orthogonal to each other.

We solved the linear algebraic problem (15) numerically, not only for the time-mean jets but also for the spin-up experiments (§ 2). The outcome, illustrated by figure 8, can be summarized as follows: The dominant barotropic and baroclinic zonal eigenmodes appear as a result of the secondary, transverse instability of the noodles, discussed in § 3.3. Such zonal eigenmodes, referred to as the primary ones, are picked up by the meridional length scale of this instability. (Note that meridional scaling in figure 5 matches meridional scaling of the zonal eigenmodes associated with the primary spectral peaks in figure 8*a*.) The zonal eigenmode spectrum is dominated by very few barotropic and baroclinic primary eigenmodes: even one or two such eigenmodes capture the velocity profiles of the zonal jets quite well (figure 8*b, c*). The barotropic zonal eigenmodes have generally larger C_n, and this is even more so in the WB flow regime, but this simply reflects the fact that the barotropic flow component is stronger than the baroclinic one.

Later in the flow spin-up process (§ 2), when the primary zonal eigenmodes reach their maximum amplitudes, the zonal-eigenmode spectrum develops secondary baroclinic- and barotropic-eigenmode peaks (e.g. as those around $n = 50$ and 80 in figure 8*a*). These peaks correspond to the emerging secondary, baroclinic and barotropic zonal eigenmodes, which have meridional length scale twice shorter than that of the primary zonal eigenmode. The secondary zonal eigenmodes are responsible for the east–west asymmetrization of the multiple jets (i.e. the eastward jets are sharper and more intense than the westward jets). We confirmed that the primary and secondary zonal eigenmodes are driven by the eddies by calculating eddy forcing (20) of the fully nonlinear solutions and by spatially correlating it with each of the zonal eigenmodes. It is found that the maximal, and also positive, correlations are indeed with the primary and secondary zonal eigenmodes.

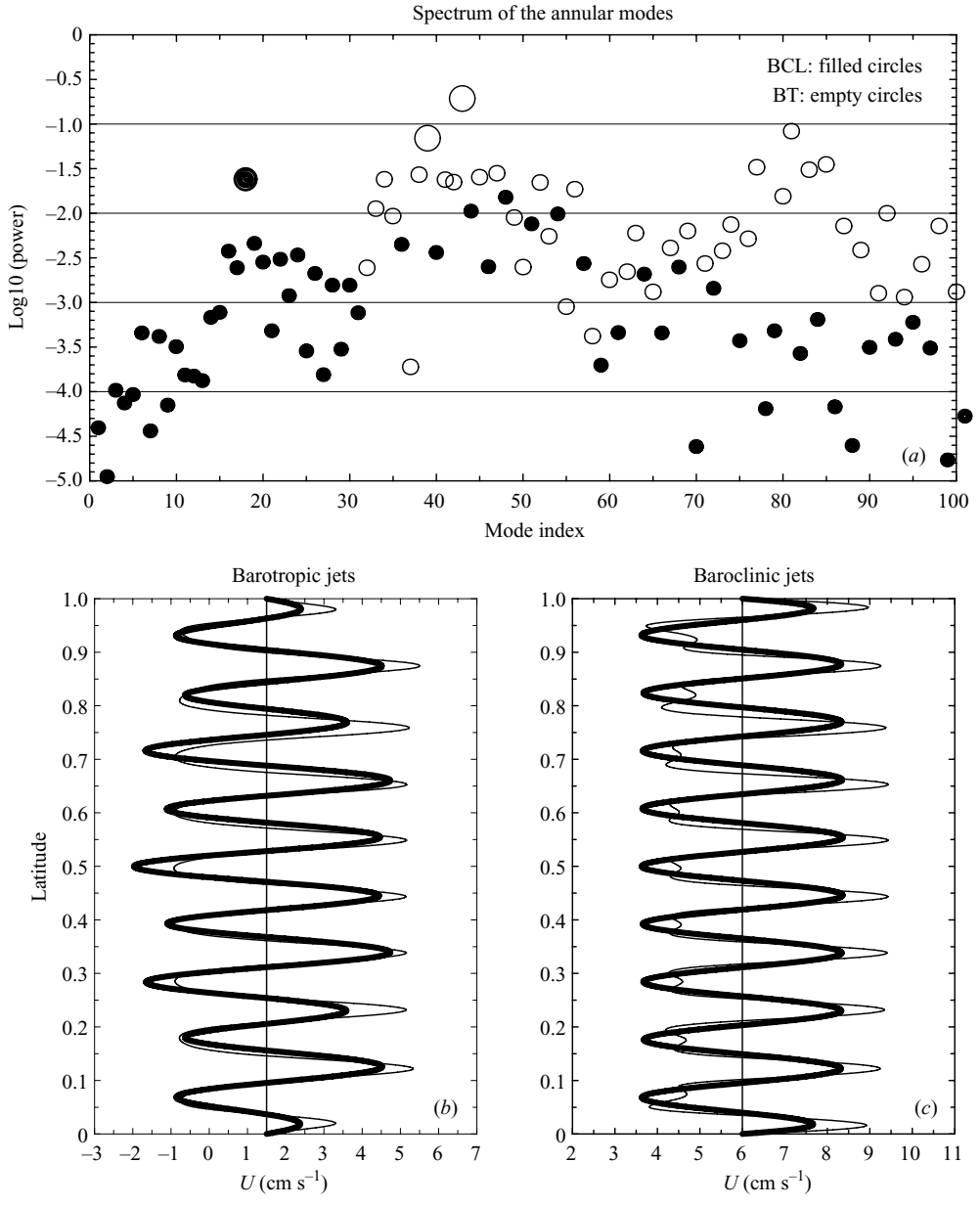

FIGURE 8. Evidence of the zonal eigenmodes in the multiple-jet flow. (*a*) Normalized spectrum of the zonal eigenmodes $P_{zon}(n)$, where n is mode index. Predominantly baroclinic/barotropic eigenmodes are indicated with the filled/empty circles. Contributions of the leading (*b*) two barotropic and (*c*) one baroclinic zonal modes (indicated by the large circles in panel *a*) to the jets are shown with thick curves, and the corresponding barotropic and baroclinic zonal velocity profiles are shown with thin curves.

To summarize, in addition to the noodles, the weakly damped zonal eigenmodes are another important aspect of the multiple-jet dynamics in the zonal channel. These eigenmodes not only provide the natural template for the multiple zonal jets but also partially meridionally localize the flow instabilities and modify the eddies, as discussed in §§ 3.5 and 3.6.

3.5. *Partial localization of the noodles*

We have demonstrated that the emergence of linear noodle mode and its subsequent instability give rise to zonal jets. In this section, we describe how the noodles are themselves modified by the emerging jets, through the mechanism of partial meridional localization, and in § 3.6 we study feedbacks of the partially localized noodles on the jets. In the zonal channel the meridional localization process is significantly amplified by the leading zonal modes in the zonal-mode spectrum (§ 3.4). By extending the linear stability analysis, we account for the feedback of the emerging zonal jets on the flow instabilities. Such extension predicts that the noodles are transformed into three distinct types of the eigenmodes – "localized noodles" – that, to a large degree, preserve long-range meridional correlations. We have calculated meridional correlations of the flow perturbations in the equilibrated state and found that these correlations are consistent with the partially localized noodles. The nonlinear self-interaction of these eigenmodes plays a central role in the jet dynamics (§ 3.6).

We take the time-mean velocity profile (i.e. imposed background flow plus time-mean zonal jets predicted by the nonlinear model) and scale its zonal-jet part with the non-dimensional amplitude, A_u, which is subsequently varied from 0 to 1.5. Thus, $A_u = 0$ corresponds to the uniform background flow (§ 3.2), and $A_u = 1$ corresponds to the actual velocity profile predicted by the nonlinear model. Since the time-mean velocity profile is nearly symmetric with respect to the middle latitude of the channel, for additional clarity we make it exactly symmetric by setting in (12)

$$u_i(y) \longrightarrow A_u\, u_i(y) \longrightarrow \frac{A_u}{2}\,[u_i(y) + u_i(L_y - y)], \tag{16}$$

where velocity is defined as in (6).

The corresponding linear stability problem is solved not only for $0 < A_u < 1.5$ but also, as a sensitivity study, for several values of ν and γ. The critical eigenmode for $A_u = 0$ corresponds to the noodles modified by the zonal boundaries (§ 2.2). The near-critical eigenmodes for $A_u = 0$ have zonal wavenumbers similar to the critical wavenumber; their meridional wavenumbers are such that they can be interpreted as meridionally elongated cells with one or two or more meridional zero crossings between the channel boundaries. We tracked the evolution of these eigenmodes, as well as the evolution of the noodle eigenmode, induced by gradually increasing A_u. The outcome is that, with increasing A_u, these eigenmodes become gradually transformed and meridionally localized on the multiple jets (figure 9).

We leave out details of the complex localization process and focus on the important aspects. One such aspect is grouping of the critical and nearly critical eigenmodes into three robust and distinct eigenmode types, discussed further below, that are well defined at large A_u (figure 9). The exact value of A_u defining the transition from the weakly perturbed noodles to the three distinct types is hard to define, but this value is significantly less than 1 and somewhere around 0.5.

A series of the full nonlinear-model simulations of the jets (not shown) for a range of eddy viscosity and bottom friction parameters showed that the structure of the jets is very robust. Below, we show that this result is consistent with the corresponding linear stability analysis. The eigenmode properties depend on both A_u and friction parameters, but at large A_u this dependence gradually fades away: when A_u approaches 1.3 – regardless of the background flow direction and friction parameters – l_{crit} and ω_{crit} converge to the universal values (figure 10). Overall, with the increasing A_u, the meridional wavelength of the critical eigenmode increases by about 30 %. The meridional wavelength tends to increase with the increasing ν and γ,

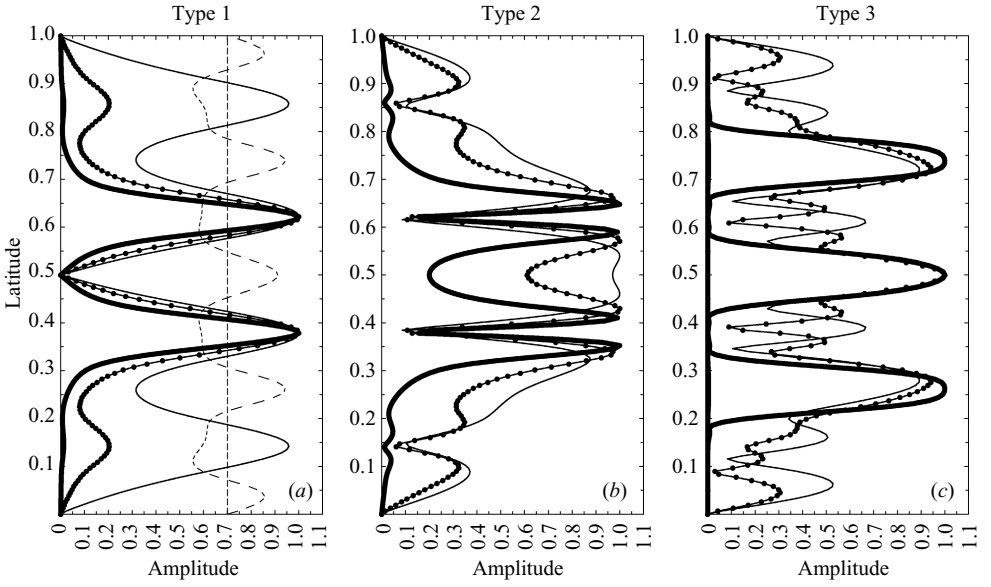

FIGURE 9. Localization of the noodles on the multiple jets. Amplitudes of the eigenmodes of (*a*) type 1, (*b*) type 2 and (*c*) type 3 are shown for amplitude of the background jets, A_u, equal to 0.2 (thin), 0.5 (thin with filled circles) and 1.5 (thick curve). On panel (*c*), three isolated peaks corresponding to $A_u = 1.5$ (thick curve) belong to three separate type 3 eigenmodes trapped by the corresponding eastward jets. (Two more eigenmodes of this sort, trapped on the near-boundary eastward jets are not shown.) EB flow is considered; and dashed curves in the panel (*a*) indicate the background and time-mean zonal velocities in the upper ocean (arbitrary units).

as in the primary stability analysis (§ 2.2). The eigenperiod decays with A_u, reaching the values of less than 1 day for A_u near 1.5, and it is sensitive to friction only in the EB flow regime with $A_u < 0.5$, where stronger friction implies a shorter eigenperiod. Finally, the eigenperiod is negative/positive in the WB/EB case, indicating that the critical eigenmode propagates to the west/east.

We focused on the 10 eigenmodes ('top 10') with the largest (and positive) growth rates, ordered them according to their growth rates and traced them over the range of A_u. The 'three types' of the eigenmodes can be characterized as the following (figures 11 and 12). The meridional structure of the eigenmodes indicates that the dynamics remain meridionally non-local for all values of A_u, although degree of this non-locality decreases with stronger jets. We checked that the existence of the "three types" of the eigenmodes does not qualitatively depend on the asymmetry between the eastward and westward jets by calculating the linear eigenmodes for a sinusoidal zonal velocity profile with similar width and amplitude of the jets.

We measure the degree of the alignment between eigenmode amplitude and jet velocity by correlating the corresponding profiles: the correlation coefficients are strongly positive/negative for the type 1 and type 3 eigenmodes and weakly negative for the type 2 eigenmodes. Thus, in terms of the amplitude, the type 1 and type 2 eigenmodes are trapped to the westward jets (i.e. prograde/retrograde jets in the WB/EB flow), and the type 3 eigenmode is trapped to the eastward (i.e. the other) jets. Also, in terms of the amplitude, all eigenmodes are meridionally symmetric with respect to the middle latitude of the channel, but in terms of the phase they are either symmetric or antisymmetric. (For A_u approaching 1.5, some of the eigenmodes split

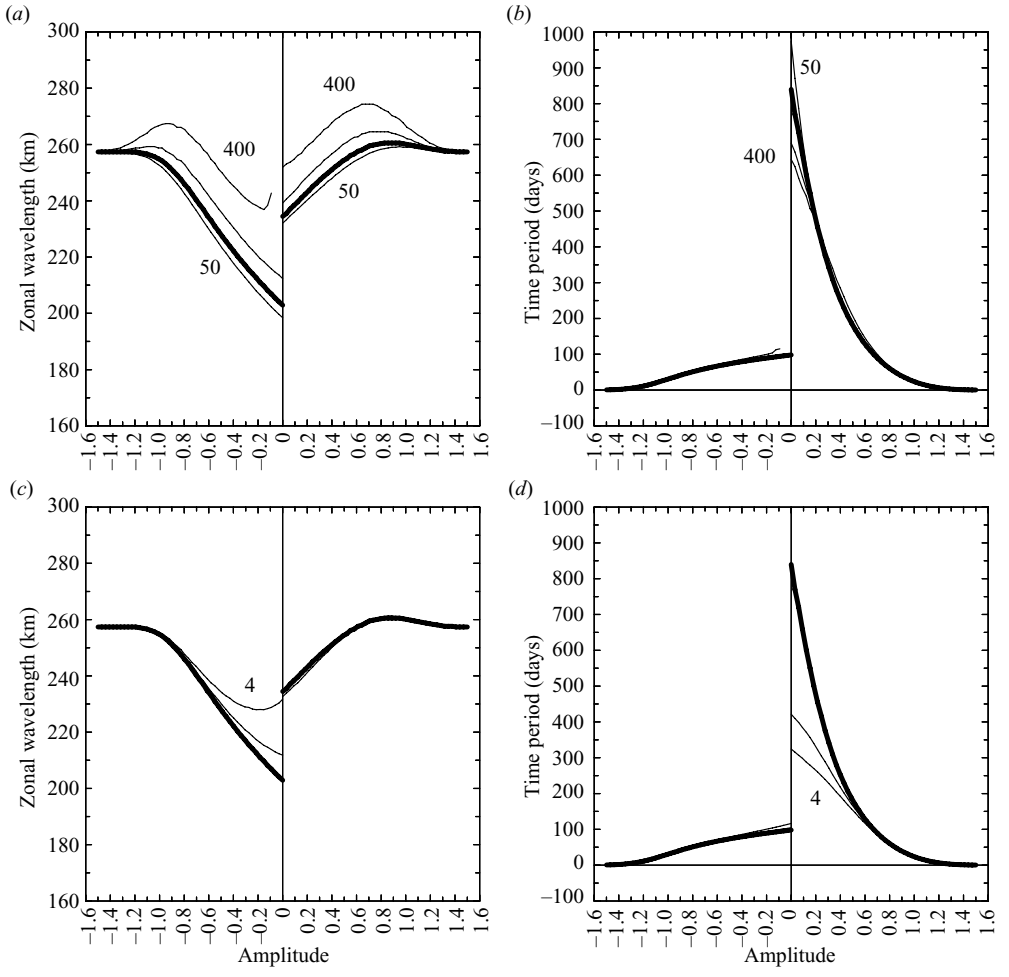

FIGURE 10. Stability properties of the multiple zonal jets. Dependence on the jets amplitude, A_u, eddy viscosity, ν, and bottom friction, γ, is explored. Left/right half of each panel corresponds to the WB/EB flow reference parameters. Upper panels show dependence on A_u of (*a*) zonal and (*b*) time periods of the critical eigenmode, for $\nu = 50$, 100, 200 and 400 m^2 s^{-1}. Left/right half of each panel corresponds to the WB/EB flow reference parameters. Amplitudes corresponding to the WB flow reference solution are indicated as $-A_u$, and amplitudes equal to the minus and plus unity correspond to the actual time-mean jets from the WB and EB flow reference solutions, respectively. Lower panels show the same properties but for $\gamma = 0$, 2 and 4×10^{-7} s^{-1}. Functions corresponding to the reference values of $\nu = 100$ m^2 s^{-1} and $\gamma = 0$ are shown with thick curves, and for clarity some curves are marked with the corresponding values of ν and γ.

in pairs that have meridionally asymmetric amplitudes, which are equivalent under the transformation $y \longrightarrow L - y$.) The westward-trapped eigenmodes are meridionally localized on the pairs of westward jets and are characterized by either two (type 1) or four (type 2) maxima of the amplitude. In the latter case, the amplitude has the characteristic 'double-hump' structure on each jet. The eastward-trapped eigenmodes also come in pairs, except for the eigenmode trapped on the central eastward jet.

The type 1 and type 2 eigenmodes can be additionally classified into subtypes 'A' and 'B' (figures 11 and 12) characterized by the meridional profile of the eigenphase

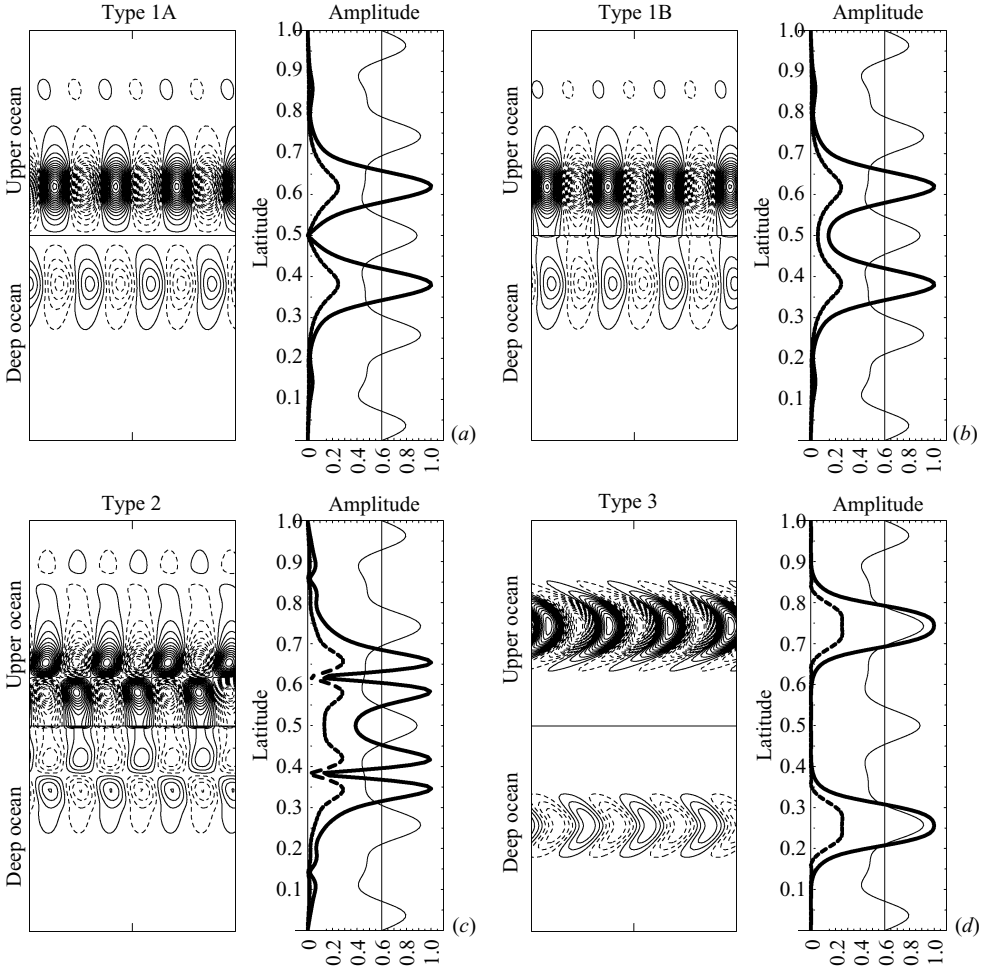

FIGURE 11. Unstable eigenmodes of the EB flow with the time-mean multiple zonal jets. Eigenmodes shown have indices (*a*) 1, (*b*) 2, (*c*) 8 and (*d*) 9, ordered in terms of the increasing decay rates. Contour plots show velocity streamfunctions of the eigenmode patterns in the 1/4-period section of the channel. Since the eigenmodes are either symmetric or antisymmetric with respect to the middle latitude of the channel, the upper-ocean pattern is shown in the northern half of the plot and the deep-ocean one in the southern half. All of the eigenmodes are normalized by the energy norm, and the (arbitrary) contour interval is the same throughout the figure. Sub-panels to the right of the contour plots show corresponding amplitudes of the upper- (thick continuous) and deep-ocean (thick dashed curve) components of the eigenmodes; the curves are normalized by the upper-ocean maximum amplitude. In each panel, thin curve with straight line in the middle show the time-mean zonal velocity profile of the jets (with arbitrary units).

that is either antisymmetric, as in subtype A, or symmetric, as in subtype B, with respect to the middle latitude of the channel. The A and B subtypes are additionally characterized by zero and non-zero amplitudes, respectively, on the eastward jets.

There are significant differences between the EB and WB flow eigenmodes – they underpin the corresponding kinematical and dynamical differences found in the nonlinear solutions. In terms of the growth rates, type 1/type 2 eigenmodes dominate in the EB/WB flows; the corresponding subtype A always dominates over

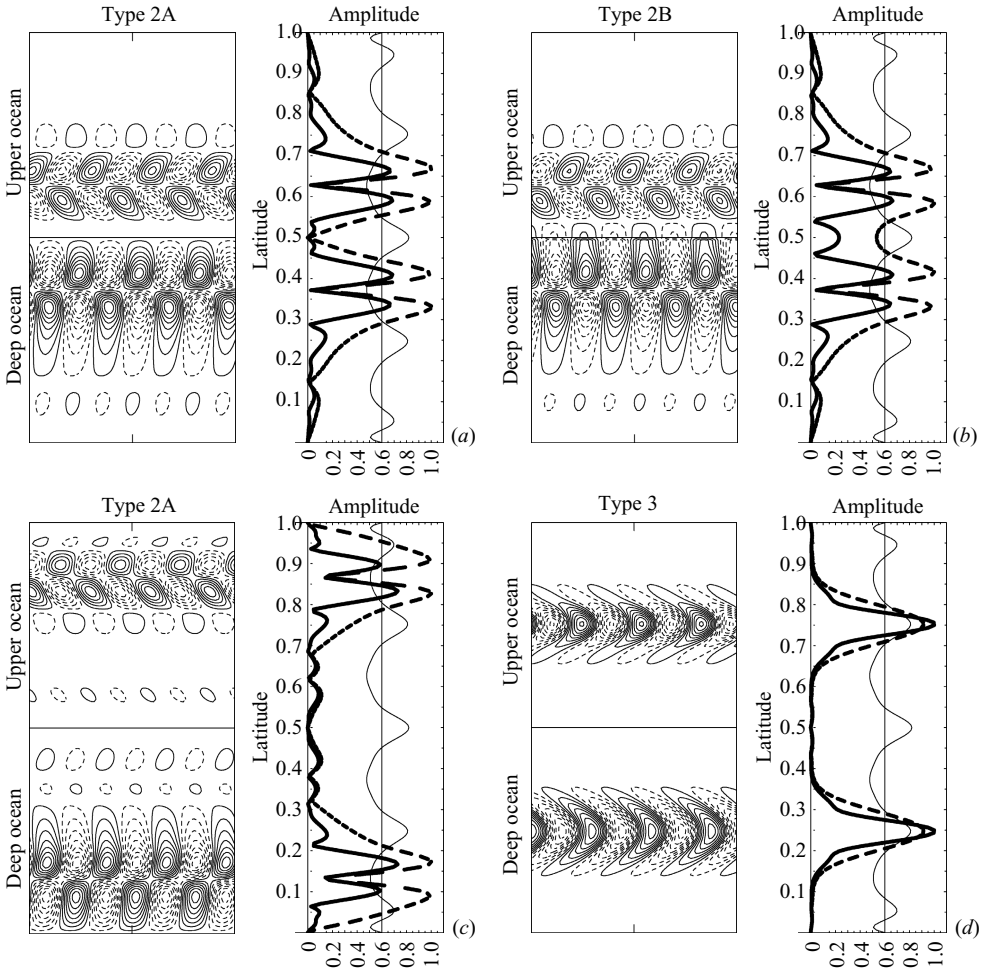

FIGURE 12. The same as figure 11 but for the WB flow. The eigenmodes shown have indices (*a*) 1, (*b*) 2, (*c*) 3 and (*d*) 7.

B. Consistent with the nonlinear analysis, the EB/WB leading eigenmodes have larger amplitudes in the upper/deep ocean. In all of the eigenmodes but substantially more so in the WB flow, there is significant vertical phase shift, which indicates intensive exchange of the potential energy between the eigenmodes and the time-mean flow. Also, in the WB flow the type 3 eigenmode amplitude is more tightly confined to the upper-ocean eastward jet cores, presumably making these jets narrower and faster, through the associated nonlinear eddy forcing. Finally, in the case of $A_u = 1$ the eigenperiods of the type 1, type 2 and type 3 eigenmodes are noticeably different: they are about 200/80, 800/100 and 100/200 days for the EB/WB flows.

To summarize, even in the presence of strong zonal jets, generation of the flow patterns with long-range meridional correlations is a very robust phenomenon. In the ocean regions populated by the multiple zonal jets, there is observational support for the noodle-like patterns. Some recent observations of the sea surface height patterns report alternating meridional jets (Sen *et al.* 2006; Huang *et al.* 2007), and qualitatively similar patterns are diagnosed from the comprehensive general circulation model

(GCM) solutions (KBP08). On the fundamental level, the noodles are characterized not so much by their particular shape but, more importantly, by the long-range meridional correlations associated with them. Identifying such correlations from the data (e.g. sea surface altimetry) would be a crucial test for the theory.

3.6. *Analysis of the multiple-jet eigenmodes*

In this section, we analyse the dynamical roles of the multiple-jet eigenmodes, discussed in the previous section. We focus on eddy forcing and its role in supporting and equilibrating the multiple jets. It is shown that the eddy forcing associated with nonlinear self-interactions of the most unstable eigenmodes, identified in the previous section, is very similar to the eddy forcing predicted by the fully nonlinear dynamics. The flow equilibration mechanism is explained in terms of the relationship between the eddy-forcing efficiency and the jet strength.

Dynamical analysis of the flow solutions is based on calculating eddy fluxes of PV and its components, relative vorticity

$$R_i = \nabla^2 \psi_i \tag{17}$$

and isopycnal stretching

$$B_1 = S_1 (\psi_2 - \psi_1), \quad B_2 = S_2 (\psi_1 - \psi_2), \tag{18}$$

which corresponds to buoyancy anomaly. First, the flow solutions are decomposed into the time-mean, $\overline{\psi_i}$, and fluctuation, ψ_i', components. In the ith isopycnal layer, the time-mean eddy PV flux is defined as

$$\overline{\boldsymbol{f}_i}(x, y) = \overline{\boldsymbol{u}_i' q_i'}, \tag{19}$$

and there are analogous R and B fluxes. In the channel, due to the zonal symmetry, the time-mean fluxes have only meridional components. The time-mean eddy forcing

$$F_i(x, y) = -\nabla \overline{\boldsymbol{f}_i} \tag{20}$$

can be interpreted as internally generated PV forcing that maintains the time-mean flow (i.e. the multiple zonal jets). In the channel, the time-mean PV balance is between eddy forcing and dissipation, and the latter always resists the jets.

The eddy forcing consists of the two physical components: convergences of $\boldsymbol{f}_R$ and $\boldsymbol{f}_B$ are the Reynolds stress forcing F_{R_i} and form stress forcing F_{B_i} respectively. The key dynamical question concerns the composition of the eddy forcing in terms of the relative vorticity and buoyancy components and in terms of the vertical-mode interactions.

First, we calculated the eddy-forcing patterns associated with the barotropic and baroclinic self-interactions of the eigenmodes (figures 13 and 14 correspond to the reference solutions) and correlated them with the corresponding PV profiles of the time-mean jets. Significant positive/negative correlation suggests that the eigenmode of interest maintains/resists the corresponding vertical-mode component of the jets (table 1). We find that the baroclinic jets are maintained by the type 1 and type 2 eddy forcings, and the barotropic jets are maintained by the type 3 eddy forcing. The baroclinic jets are resisted by the type 3 eddy forcing and substantially more so in the WB flow. The barotropic jets are weakly resisted by the type 1 eddy forcing, and the type 2 eddy forcing resists them only in the EB flow.

Regardless of the background flow direction, the barotropic jets are maintained by the same type 3 eigenmode. This result explains the similarity of the eddy forcings in the fully nonlinear, barotropic-mode dynamics of the EB and WB flows. Also, the type

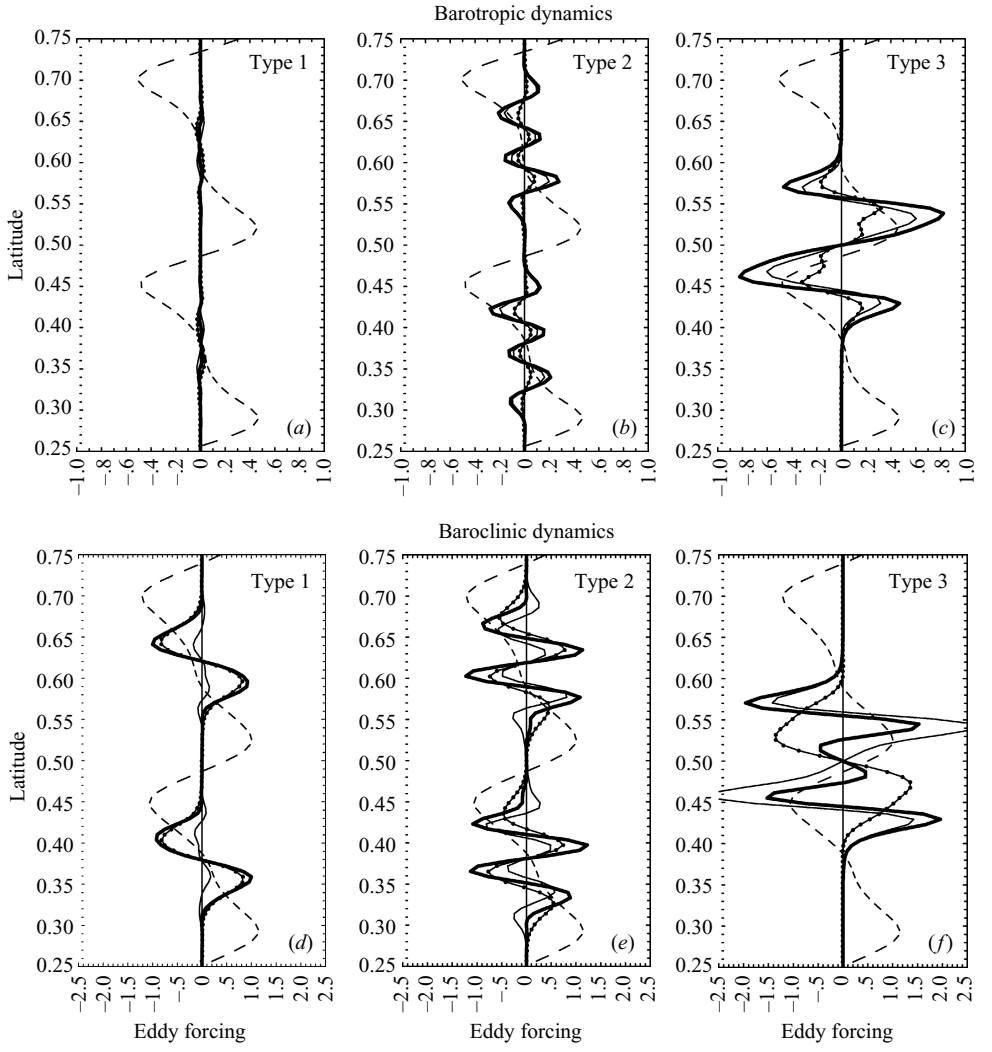

FIGURE 13. Eddy forcing and its components of the meridionally localized eigenmodes: EB flow. Upper row of panels corresponds to the barotropic eddy forcing of the gravest eigenmodes localized in the centre of the channel: (*a*) type 1, (*b*) type 2 and (*c*) type 3 eigenmodes. Upper row of panels: full eddy forcing (thick), as well as its barotropic–barotropic (thin) and baroclinic–baroclinic (thin with filled circles) components are shown. Lower row of panels: full eddy forcing (thick), as well as its Reynolds stress (thin) and form stress (thin with filled circles) forcing components are shown. The corresponding time-mean PV anomalies are shown with dashed curve (arbitrary value). Each eddy forcing curve is normalized by the maximum absolute value of the eddy forcing corresponding to the gravest eigenmode.

3 eddy forcing has equally important barotropic–barotropic and baroclinic–baroclinic components that are qualitatively similar to those predicted by the nonlinear model. The baroclinic jets can be maintained by either type 1 or type 2 eddy forcing, depending on whether type 1 or type 2 eigenmode has the fastest growth rate. This fact makes direction of the background flow crucial: as shown in the previous section, type 1/type 2 eddy forcing dominates the EB/WB flow regime. Since the type 2 eddy forcing is characterized by the presence of the high-frequency meridional oscillation,

	EB: $A_u =$ 0.7	EB: $A_u =$ 1.0	EB: $A_u =$ 1.3	WB: $A_u =$ 0.7	WB: $A_u =$ 1.0	WB: $A_u =$ 1.3
Type 1: BT	−0.08	−0.02	−0.01	−0.06	−0.05	−0.02
Type 1: BCL	+0.24	+0.17	+0.13	+0.33	+0.30	+0.23
Type 2: BT	−0.19	−0.07	−0.06	+0.02	+0.01	+0.01
Type 2: BCL	+0.23	+0.16	+0.10	+0.14	+0.18	+0.19
Type 3: BT	+0.40	+0.29	+0.23	+0.34	+0.22	+0.19
Type 3: BCL	+0.01	−0.02	−0.04	−0.22	−0.14	−0.31

TABLE 1. Projection on the time-mean jets of the eddy forcing associated with critical eigenmodes of the meridionally localized types. Correlation values labelled by BT/BCL correspond to the barotropic/baroclinic dynamics; labels EB and WB indicate direction of the background flow; and parameter A_u indicates strength of the multiple jets.

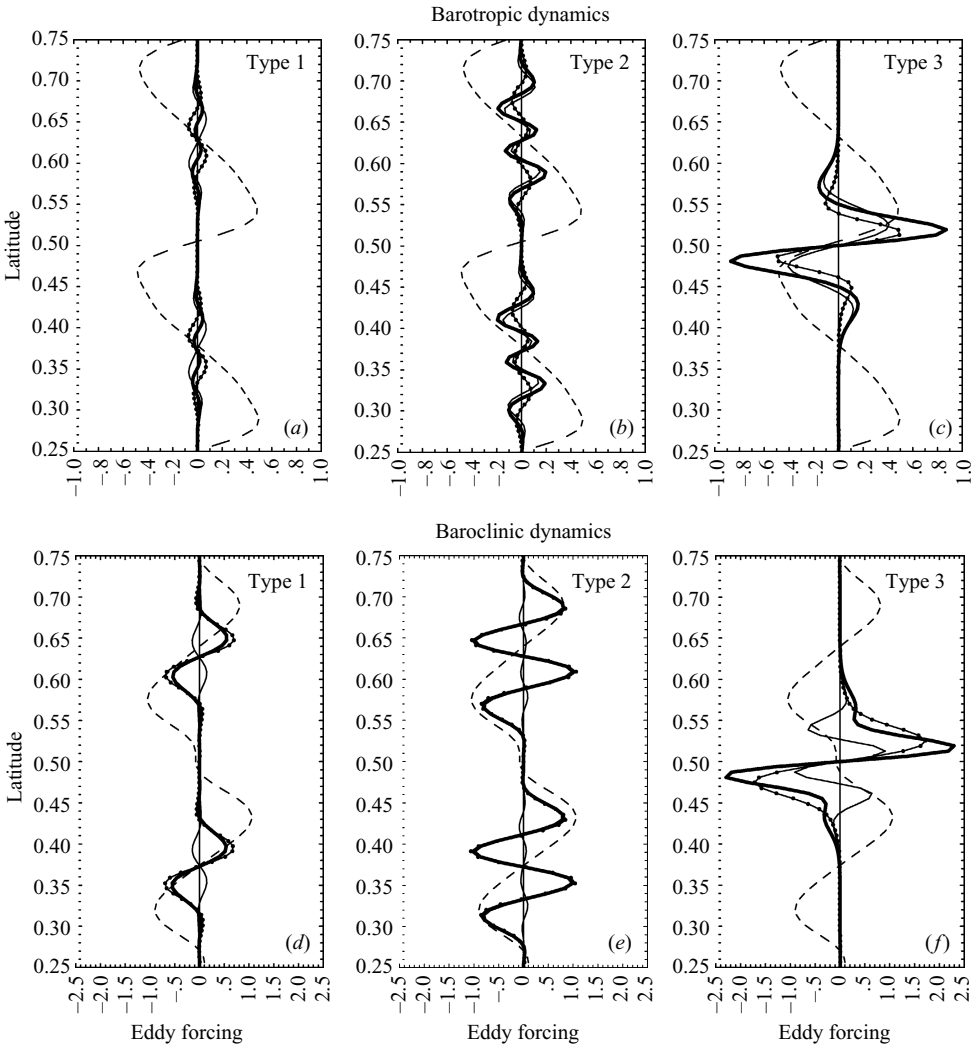

FIGURE 14. The same as figure 13 but for the WB flow.

it explains the similar property of the corresponding, fully nonlinear eddy forcing (not shown).

Important differences between the eigenmode-induced eddy forcings in the EB and WB flows (figures 13 and 14) explain the following key aspects of the dynamics: In the EB flow, the nonlinear baroclinic dynamics is such that the Reynolds and form stress forcings significantly balance each other, and the former maintains the jets (this result was originally obtained in P93). The linear eigenmode analysis not only confirms these dynamical properties but also provides some insight, as it turns out that the properties are a result of the collective action of all three types of the eigenmodes. We find that the Reynolds stress forcing contribution comes solely from the type 3 eigenmode, whereas the other eigenmodes provide weak Reynolds stress forcings that are poorly correlated with the jets. The type 3 form stress forcing resists the jets very efficiently, but its effect is partially cancelled by the type 1 and type 2 form stress forcings. Thus, the baroclinic jets are explained by the collective jet-maintaining action of the type 1 and type 2 form stress forcings and the type 3 Reynolds stress forcing; their action is resisted by the type 3 form stress forcing. In other words, the eastward jets are more baroclinically unstable rather than 'negatively viscous' (Starr 1968), but the baroclinic instability effect is substantially compensated by the jet-driving buoyancy fluxes in the westward jets.

In the WB flow, the nonlinear baroclinic dynamics is such that the form stress forcing maintains the jets, and the Reynolds stress forcing resists them. The eigenmode analysis suggests that the weak jet-resisting Reynolds stress forcing and the strong jet-maintaining form stress forcing are associated with the type 1 and type 2 eigenmodes. However, both the Reynolds and form stress eddy forcings associated with the type 3 eigenmode tend to partially compensate for the above effects. Thus, the eastward jets are just baroclinically unstable, whereas the counteracting 'negative viscosity' effect is present but rather weak; and the westward jets provide the jet-maintaining form stress forcing.

What is the mechanism that bounds the growth of the jets and equilibrates the flow? Below, we demonstrate that this mechanism has a simple explanation in terms of the structural changes of the eigenmodes that are associated with transient situations when the jets are weaker or stronger than on the average. This equilibration mechanism is complementary to some others, which are based on the weakly nonlinear triad interactions (Pedlosky 1975*a, b*) and on nonlinear Lyapunov stability arguments (Shepherd 1988).

To find this, first, we defined a measure of strength of the multiple jets as the meridional average of zonally averaged zonal velocity $\tilde{u}$:

$$\Sigma^{(i)}(t) = \frac{1}{L_y} \int_0^{L_y} |\tilde{u}^{(i)}(t, y)| \, \mathrm{d}y, \tag{21}$$

where the superscript denotes the vertical mode. Then, we calculated probability density functions (p.d.f.s) of $\Sigma^{(i)}$ and found that the corresponding variances in the EB regime are about $\pm 2\,\%$ of the time mean $\overline{\Sigma^{(i)}}$, and in the WB regime they are about $\pm 5\,\%$ and $\pm 9\,\%$ of $\overline{\Sigma^{(1)}}$ and $\overline{\Sigma^{(2)}}$, respectively. All p.d.f.s are characterized by single-maximum bell-shaped curves (not shown). We also calculated time series $\Upsilon^{(i)}(t)$ of correlation between instantaneous zonally averaged meridional profiles of the PV anomaly and the corresponding eddy forcing. We verified that $\Upsilon^{(i)}(t)$ is highly and positively correlated with $\mathrm{d}\Sigma^{(i)}(t)/\mathrm{d}t$, confirming that the jets are amplified, when the eddy forcing has significant projection on them. In other words, $\Upsilon^{(i)}(t)$ is the measure

of efficiency of eddy-forcing action on the jets; when eddy forcing is highly efficient, it amplifies the jets.

We also diagnosed time series of the total eddy energy of the flow, by defining eddies as fluctuations around instantaneous zonally averaged flow. Then, we focused on the conditional states when flow is either weaker (i.e. weak state, $\Sigma < \overline{\Sigma}$) or stronger (i.e. strong state, $\Sigma > \overline{\Sigma}$) than the average. When instantaneous weak/strong flow is accelerated/decelerated, we say that it is driven toward the average; if the opposite is true, then the flow is driven away from the average. In the EB flow, we find that when barotropic/baroclinic component of the jets is driven toward the average, correlation of its eddy forcing with the jets changes by about 3 %/20 %. That is in the weak state eddy forcing is more efficient, and in the strong state it is *less efficient*. In the WB flow, the situation is similar, and the corresponding correlation changes are about 5 % and 35 % for the barotropic and baroclinic components of the jets, respectively. On the other hand, in both EB and WB flows, the corresponding change of the eddy energy is about 2 %: the energy is larger in the weak state and smaller in the strong state. Relatively small change of the eddy energy suggests that equilibration is achieved mostly due to the change of the eddy-forcing efficiency rather than intensity.

The change of the eddy-forcing efficiency is simply explained in terms of the meridionally localized linear eigenmodes (table 1). Around the flow equilibrium, stronger jets result in more meridionally localized eddy forcing associated with the eigenmodes (figures 13 and 14), and such forcing becomes less correlated with the jets and, therefore, less efficient. The only exception is the baroclinic type 2 eddy forcing in the WB flow, but its effect is strongly overcome by contributions of the other eigenmodes.

To summarize, analysis of the multiple-jet linear eigenmodes yields insights into the fully nonlinear dynamics. The underlying linear eigenmodes can be viewed as descendants of the primary and secondary instability patterns that are distorted and partially localized on the jets. In particular, analysis of the eigenmode-induced eddy forcing explains the relative roles of the relative-vorticity and buoyancy eddy fluxes in maintaining and resisting the jets. Also, this analysis explains some aspects of the mechanism of the flow equilibration, but so far it does not predict the rate of energy dissipation, the eddy heat flux and other important statistical properties of the equilibrated state.

4. Conclusions and discussion

We focused on a fairly simple, multi-layer quasi-geostrophic model configured in a zonal channel and driven by the imposed zonal background flow with vertical shear. This is a classical model for the multiple zonal jets, such as those in the atmospheres of giant gas planets (e.g. Haidvogel & Held 1980; Panetta 1993). Although the model is idealized, as dictated by our theoretical approach, it is motivated by the oceanic flows (e.g. nearly zonal flows in mid-latitude gyres, where the background mean flow is either eastward or westward, and the Antarctic Circumpolar Current). Our study connects the EB and WB flow regimes, and finds the mechanism that explains jet formation in both of them. The WB flow has never been looked at in the past, and we find that its multiple-jet dynamics is significantly different from that in the EB flow. We carry out full nonlinear-model calculations and, then, focus on the linear stability analysis of the obtained flow and its components. The results of the linear analysis are verified against the fully nonlinear results (Berloff *et al.* 2009).

It is commonly thought that the meridional scaling of the jets is the length scale at which the inverse energy cascade, typical for the two-dimensional turbulence, is 'arrested' by propagating Rossby waves, so that the energy becomes directed into multiple zonal jets. We dispute this conjecture by arguing that the energy efficiently overcomes the 'arrest', as it goes directly from the unstable background flow into the alternating meridional jets, that is the noodles. This pattern is consistent with the arguments of the baroclinic instability theory that the direction perpendicular to the mean flow corresponds to the motions that most efficiently extract energy from the background flow (Pedlosky 1987).

The noodles emerge to finite amplitude and, then, experience the secondary, transverse instability that sets meridional scale of the jets. In the channel, this instability efficiently projects on the corresponding zonal linear eigenmode, which is also weakly damped. This eigenmode emerges and contributes to the multiple jets. Emerging multiple jets feed back on the primary and secondary instabilities through the partial localization mechanism that produces three types of the unstable eigenmodes. Analysis of these eigenmodes and their nonlinear self-interactions yields significant insights into the flow dynamics. In particular, it explains interactions between the vertical modes of the flow and roles of the Reynolds and form stress forcings in the dynamics. Next, we find that meridional localization of instabilities also provides bounding mechanism responsible for equilibration of the multiple jets. Despite many complicating physical factors neglected in the idealized model, the noodle solutions are remarkably similar to the analogous patterns seen in the ocean observations and comprehensive eddy-resolving models (Huang *et al.* 2007).

Our results imply that there is no simple and universal scaling for the meridional jet scale, because instabilities that generate the jets should depend on the vertical and horizontal structures of the background flow (e.g. as previously suggested by Manfroi & Young 2002 for simpler flows). This finding is further supported by Berloff *et al.* (2009), who report disagreement between the Rhines scaling and the jet width in a wide range of parameters. On the other hand, we argue that the jet scale can be predicted by the linear stability analysis – this point of view is in the sharp contrast with the nonlinear inverse cascade arguments.

The linear stability analysis of the equilibrated multiple jets makes several predictions, which are consistent with the fully nonlinear dynamics (Berloff *et al.* 2009). In particular, the barotropic component of the jets is maintained by both barotropic–barotropic and baroclinic–baroclinic interactions. In the EB flow, the baroclinic component of the jets is maintained by the Reynolds stress forcing and resisted by the form stress forcing. The former is an example of 'negative viscosity' phenomena (Phillips 1956; Starr 1968), and the latter is manifestation of the baroclinic instability. More thorough analysis reveals that the eastward (prograde) jets are baroclinically unstable rather than 'negatively viscous', but the baroclinic instability effect is substantially compensated by the jet-driving buoyancy fluxes in the westward jets.

In the WB flow, the Reynolds stress forcing resists and the form stress forcing maintains the jets. Hence, the jets are maintained locally by the process which is opposite to the baroclinic instability (in the sense that the eddies release their potential energy back to the mean flow) and opposed by the effective eddy viscosity. In this case, the eastward (retrograde) jets are just baroclinically unstable, whereas their counteracting 'negative viscosity' effect is present but rather weak; the westward jets provide the jet-maintaining form stress forcing.

The simple model we have presented here needs to be extended in the future. In particular, the extension of our analysis to closed-basin models should focus

on the formation of the multiple jets in mid-latitude gyres and on the effects of spatial inhomogeneity of the background flow. These inhomogeneities, deliberately neglected in this study, can impose their own length scales and change significantly the underlying dynamics. In particular, non-zonality of the background flow can significantly boost generation of the eddies (Pedlosky 1987; Spall 2000) and change their structure (Kamenkovich & Pedlosky 1996). Also, horizontal shear can become a significant source of PV. Furthermore, a recent study by Hristova, Pedlosky & Spall (2008) suggests that multiple zonal jets can be generated by instability of the purely meridional, horizontally uniform and vertically sheared flow, and the connection of that work to the present study needs to be clarified. With our model we do not find meridional PV 'staircase' proposed in several more idealized studies (e.g. Dritschel & McIntyre 2008), and this issue is discussed in details in Berloff *et al.* (2009). Finally, calculation of the spectrum of the eigenmodes directly from the fully nonlinear solutions can provide further insight into the flow equilibration process as well as into the kinematics of mixing across and along the jets.

Funding for PB was provided by NSF grants OCE 0344094 and OCE 0725796 and by the research grant from the Newton Trust of the University of Cambridge. Funding for IK was provided by NSF grants OCE 0346178 and 0749722. Funding for JP was provided by NSF grant OCE 0451086. We are grateful for the constructive comments of the anonymous reviewers that led to significant improvement of this paper.

Appendix. Linear stability problem

Here, we discuss formulation of the two-layer linear stability problem. In the situation with a uniform shear and the unbounded domain, given Fourier transform of the perturbation streamfunction

$$\psi_i \longrightarrow \psi_i \exp[\mathrm{i}(kx + ly - \omega t)] \tag{A 1}$$

the following linearized equations are obtained:

$$\begin{aligned}\omega[-(k^2+l^2+S_1)\psi_1 + S_1\psi_2] = {} & \psi_1\,[-kU_1(k^2+l^2) + k(\beta - S_1U_2) \\ & + \mathrm{i}\nu(k^4 + 2k^2l^2 + l^4)] + \psi_2\,[kS_1U_1], \qquad \text{(A 2)}\\ \omega[S_2\psi_1 - (k^2+l^2+S_2)\psi_2] = {} & \psi_1\,[kS_2U_2] + \psi_2\,[-kU_2(k^2+l^2) + k(\beta - S_2U_1) \\ & + \mathrm{i}\nu(k^4 + 2k^2l^2 + l^4) + \mathrm{i}\gamma(k^2+l^2)]. \qquad \text{(A 3)}\end{aligned}$$

Non-trivial solutions of the above pair of the equations require that the determinant of the coefficients of ψ_i is zero. This statement yields the dispersion relationship between k, l and ω.

In the zonal channel with either uniform or non-uniform shear, $U_i(y)$, given Fourier transform in the zonal direction

$$\psi_i \longrightarrow \psi_i(y) \exp[\mathrm{i}(kx - \omega t)] \tag{A 4}$$

the linearized equations are

$$\begin{aligned}\omega[\psi_1'' - (k^2+S_1)\psi_1 + S_1\psi_2] = {} & \mathrm{i}\nu\psi_1^{IV} + [k(U_1 - \mathrm{i}2\nu)]\psi_1'' + [k(\beta - k^2U_1 - U_1'' - S_1U_2) \\ & + \mathrm{i}\nu k^4]\psi_1 + [kS_1U_1]\psi_2, \qquad \text{(A 5)}\\ \omega[\psi_2'' - (k^2+S_2)\psi_2 + S_2\psi_1] = {} & \mathrm{i}\nu\psi_2^{IV} + [k(U_2 - \mathrm{i}2\nu) - \mathrm{i}\gamma]\psi_2'' + [k(\beta - k^2U_2 - U_2'' \\ & - S_2U_1) + l\mathrm{i}(\nu k^4 + \gamma k^2)]\psi_2 + [kS_2U_2]\psi_1. \qquad \text{(A 6)}\end{aligned}$$

The above equations are discretized with finite differences and solved numerically.

In the unbounded domain with a uniform zonal shear U_i and periodic meridional jets with finite amplitude $V_i(x)$ we apply Fourier transform in the meridional direction:

$$\psi_i \longrightarrow \psi_i(x)\exp[\mathrm{i}(ly - \omega t)]. \tag{A 7}$$

We look for $\psi_i(x)$ that is periodic over the domain that includes eight meridional jets.

REFERENCES

Baldwin, M., Rhines, P., Huang, H.-P. & McIntyre, M. 2007 The jet-stream conundrum. *Science* **315**, 467–468.

Balk, A., Nazarenko, S. & Zakharov, V. 1990 On the nonlocal turbulence of drift type waves. *Phys. Rev. Lett.* A **146**, 217–221.

Berloff, P. 2005 On rectification of randomly forced flows. *J. Mar. Res.* **63**, 497–527.

Berloff, P., Kamenkovich, I. & Pedlosky, J. 2009 A model of multiple zonal jets in the oceans: dynamical and kinematical analysis. *J. Phys. Oceanogr*, submitted.

Bonfigli, G. & Kloker, M. 2005 Secondary instability of crossflow vortices: validation of the stability theory by direct numerical simulation. *J. Fluid Mech.* **583**, 229–272.

Chekhlov, A., Orszag, S., Sukoriansky, S., Galperin, B. & Staroselsky, I. 1996 The effect of small-scale forcing on large-scale structures in two-dimensional flows. *Physica* D **98**, 321–334.

Danilov, S. & Gryanik, V. 2004 Barotropic beta-plane turbulence in a regime with strong zonal jets revisited. *J. Atmos. Sci.* **61**, 2283–2295.

Danilov, S. & Gurarie, D. 2004 Scaling, spectra and zonal jets in beta-plane turbulence. *Phys. Fluids* **16**, 2592–2603.

Dritschel, D. & McIntyre, M. 2008 Multiple jets as PV staircases: the Phillips effect and the resilience of eddy-transport barriers. *J. Atmos. Sci.* **65**, 855–874.

Farrell, B. & Ioannou, P. 2007 Structure and spacing of jets in barotropic turbulence. *J. Atmos. Sci.* **64**, 3652–3665.

Farrell, B. & Ioannou, P. 2008 Formation of jets by baroclinic turbulence. *J. Atmos. Sci.* **65**, 3353–3375.

Galperin, B., Nakano, H., Huang, H. & Sukoriansky, S. 2004 The ubiquitous zonal jets in the atmospheres of giant planets and Earth's oceans. *Geophys. Res. Lett.* **31**, L13303.

Haidvogel, D. & Held, I. 1980 Homogeneous quasi-geostrophic turbulence driven by a uniform temperature gradient. *J. Atmos. Sci.* **37**, 2644–2660.

Herbei, R., McKeague, I. & Speer, K. 2008 Gyres and jets: inversion of tracer data for ocean circulation structure. *J. Phys. Oceanogr.* **38**, 1180–1202.

Hogg, N. & Owens, B. 1999 Direct measurement of the deep circulation within the Brazil basin. *Deep-Sea Res.* **46**, 335–353.

Hristova, H., Pedlosky, J. & Spall, M. 2008 Radiating instability of a meridional boundary current. *J. Phys. Oceanogr.* **38**, 2294–2307.

Huang, H.-P., Kaplan, A., Curchitser, E. & Maximenko, N. 2007 The degree of anisotropy for mid-ocean currents from satellite observations and an eddy-permitting model simulation. *J. Geophys. Res.* **112**, C09005.

Huang, H.-P. & Robinson, W. 1998 Two-dimensional turbulence and persistent zonal jets in a global barotropic model. *J. Atmos. Sci.* **55**, 611–632.

Ivanov, L., Collins, C. & Margolina, T. 2008 System of quasi-zonal jets off California revealed from satellite altimetry. *Geophys. Res. Lett.* **36**, L03609.

Kamenkovich, I., Berloff, P. & Pedlosky, J. 2009 Role of eddy forcing in the dynamics of zonal jets in the North Atlantic. *J. Phys. Oceanogr.* in press.

Kamenkovich, I. & Pedlosky, J. 1996 Radiating instability of nonzonal ocean currents. *J. Phys. Oceanogr.* **26**, 622–643.

Kaspi, I. & Flierl, G. 2007 Formation of jets by baroclinic instability on gas planet atmospheres. *J. Atmos. Sci.* **64**, 3177–3194.

Kramer, W., van Buren, M., Clercx, H. & van Heijst, G. 2006 Beta-plane turbulence in a basin with no-slip boundaries. *Phys. Fluids* **18**, 026603.

Lee, S. 1997 Maintenance of multiple jets in a baroclinic flow. *J. Atmos. Sci.* **54**, 1726–1738.

Manfroi, A. & Young, W. 1999 Slow evolution of zonal jets on the beta plane. *J. Atmos. Sci.* **56**, 784–800.

Manfroi, A. & Young, W. 2002 Stability of β-plane Kolmogorov flow. *Physica* D **162**, 208–232.

Maximenko, N., Bang, B. & Sasaki, H. 2005 Observational evidence of alternating zonal jets in the world ocean. *Geophys. Res. Lett.* **32**, L12607.

Maximenko, N., Melnichenko, O., Niiler, P. & Sasaki, H. 2008 Stationary mesoscale jet-like features in the ocean. *Geophys. Res. Lett.* **35**, L08603.

McIntyre, M. 1982 How well do we understand the dynamics of stratospheric warmings? *J. Meteorol. Soc. Jpn* **60**, 37–65.

McWilliams, J. 1977 A note on a consistent quasigeostrophic model in a multiply connected domain. *Dyn. Atmos. Oceans* **1**, 427–441.

McWilliams, J. 2006 *Fundamentals of Geophysical Fluid Dynamics.* Cambridge University Press, p. 249.

Nadiga, B. 2006 On zonal jets in oceans. *Geophys. Res. Lett.* **33**, L10601.

Nakano, H. & Hasumi, H. 2005 A series of zonal jets embedded in the broad zonal flows in the Pacific obtained in eddy-permitting ocean general circulation models. *J. Phys. Oceanogr.* **35**, 474–488.

Ollitrault, M., Lankhorst, M., Fratantoni, D. & Richardson, P. 2006 Zonal intermediate currents in the equatorial Atlantic Ocean. *Geophys. Res. Lett.* **33**, L05605.

Orszag, S. & Patera, A. 1983 Secondary instability of wall-bounded shear flows. *J. Fluid Mech.* **128**, 347–385.

Panetta, L. 1993 Zonal jets in wide baroclinically unstable regions: persistence and scale selection. *J. Atmos. Sci.* **50**, 2073–2106.

Pedlosky, J. 1975*a* The amplitude of baroclinic wave triads and mesoscale motion in the ocean. *J. Phys. Oceanogr.* **5**, 608–614.

Pedlosky, J. 1975*b* On secondary baroclinic instability and the meridional scale of motion in the ocean. *J. Phys. Oceanogr.* **5**, 603–607.

Pedlosky, J. 1987 *Geophysical Fluid Dynamics*, 2nd edn. Springer, p. 710.

Phillips, N. 1956 The general circulation of the atmosphere: a numerical experiment. *Quart. J. R. Meteorol. Soc.* **82**, 123–164.

Qiu, B., Scott, R. & Chen, S. 2008 Length scales of eddy generation and nonlinear evolution of the seasonally-modulated South Pacific subtropical countercurrent. *J. Phys. Oceanogr.* **38**, 1515–1528.

Rhines, P. 1975 Waves and turbulence on a beta-plane. *J. Fluid Mech.* **69**, 417–443.

Richards, K., Maximenko, N., Bryan, F. & Sasaki, H. 2006 Zonal jets in the Pacific ocean. *Geophys. Res. Lett.* **33**, L03605.

Schlax, M. & Chelton, D. 2008 The influence of mesoscale eddies on the detection of quasi-zonal jets in the ocean. *Geophys. Res. Lett.* **35**, L24602.

Sen, A., Arbic, B., Scott, R., Holland, C., Logan, E. & Qiu, B. 2006 Persistent small-scale features in maps of the anisotropy of ocean surface velocities: implications for mixing? *Eos. Trans. AGU* **87** (52).

Shepherd, T. 1988 Nonlinear saturation of baroclinic instability. Part 1. The two-layer model. *J. Atmos. Sci.* **45**, 2014–2025.

Sinha, B. & Richards, K. 1999 Jet structure and scaling in Southern Ocean models. *J. Phys. Oceanogr.* **29**, 1143–1155.

Smith, K. 2004 A local model for planetary atmospheres forced by small-scale convection. *J. Atmos. Sci.* **61**, 1420–1433.

Sokolov, S. & Rintoul, S. 2007 Multiple jets of the Antarctic Circumpolar Current south of Australia. *J. Phys. Oceanogr.* **37**, 1394–1412.

Spall, M. 2000 Generation of strong mesoscale eddies by weak ocean gyres. *J. Mar. Res.* **58**, 97–116.

Starr, V. 1968 *Physics of Negative Viscosity Phenomena.* McGraw-Hill, p. 256.

Stern, M. & Simeonov, J. 2005 The secondary instability of salt fingers. *J. Fluid Mech.* **533**, 361–380.

Sukoriansky, S., Dikovskaya, N. & Galperin, B. 2007 On the 'arrest' of inverse energy cascade and the Rhines scale. *J. Atmos. Sci.* **64**, 3312–3327.

Theiss, J. 2004 Equatorward energy cascade, critical latitude, and the predominance of cyclonic vortices in geostrophic turbulence. *J. Phys. Oceanogr.* **34**, 1663–1678.

Thompson, A. & Young, W. 2007 Baroclinic eddy heat fluxes: zonal flows and energy balance. *J. Atmos. Sci.* **64**, 3214–3231.

Treguier, A. & Panetta, L. 1994 Multiple zonal jets in a quasigeostrophic model of the Antarctic Circumpolar Current. *J. Phys. Oceanogr.* **24**, 2263–2277.

Vallis, G. & Maltrud, M. 1993 Generation of mean flows and jets on a beta plane and over topography. *J. Phys. Oceanogr.* **23**, 1346–1362.

Williams, G. 1978 Planetary circulations. Part 1. Barotropic representation of jovian and terrestrial turbulence. *J. Atmos. Sci.* **35**, 1399–1426.